

# bradscholars

## Flexural behavior of ECC–concrete hybrid composite beams reinforced with FRP and steel bars

Item Type	Article
Authors	Ge, W-J.;Ashour, Ashraf;Yu, J.;Gao, P.;Cao, D-F.;Cai, C.;Ji, X.
Citation	Ge W-J, Ashour AF, Yu J et al (2019) Flexural behavior of ECC–concrete hybrid composite beams reinforced with FRP and steel bars. Journal of Composites for Construction. 23(1): 04018069.
DOI	<a href="https://doi.org/10.1061/(ASCE)CC.1943-5614.0000910">https://doi.org/10.1061/(ASCE)CC.1943-5614.0000910</a>
Rights	©2018 American Society of Civil Engineers. This material may be downloaded for personal use only. Any other use requires prior permission of the American Society of Civil Engineers. This material may be found at <a href="https://doi.org/10.1061/(ASCE)CC.1943-5614.0000910">https://doi.org/10.1061/(ASCE)CC.1943-5614.0000910</a> .
Download date	2026-04-14 22:10:09
Link to Item	<a href="http://hdl.handle.net/10454/16536">http://hdl.handle.net/10454/16536</a>

# Experimental study on the flexural behavior of ECC-concrete hybrid composite beams reinforced with FRP and steel bars

Wen-Jie Ge<sup>1\*</sup>, Ashraf F. Ashour<sup>2</sup>, Jiamin Yu<sup>3</sup>, Peiqi Gao<sup>4</sup>, Da-Fu Cao<sup>5</sup>, Chen Cai<sup>6</sup>, Xiang Ji<sup>7</sup>

(1. Ph.D., Associate Professor, College of Civil Science and Engineering, Yangzhou University, Yangzhou 225127, China(corresponding author), E-mail: gewj@yzu.edu.cn; 2. Ph.D., Professor, School of Engineering, University of Bradford, Bradford, BD7 1DP, UK; 3. M.S. Candidate, College of Civil Science and Engineering, Yangzhou University, Yangzhou 225127, China; 4. M.S. Candidate, College of Civil Science and Engineering, Yangzhou University, Yangzhou 225127, China; 5. M.S., Professor, College of Civil Science and Engineering, Yangzhou University, Yangzhou 225127, China 6; M.S. Candidate, College of Civil Science and Engineering, Yangzhou University, Yangzhou 225127, China; 7. M.S. Candidate, College of Civil Science and Engineering, Yangzhou University, Yangzhou 225127, China.)

**Abstract:** This paper aims to investigate the flexural behavior of engineered cementitious composite (ECC)-concrete hybrid composite beams reinforced with fiber reinforced polymer (FRP) bars and steel bars. Thirty two hybrid reinforced composite beams having various ECC height replacement ratio and combinations of FRP and steel reinforcements were experimentally tested to failure in flexure. Test results showed that cracking, yield and ultimate moments as well as the stiffness of hybrid and ECC beams are improved compared with traditional concrete beams having the same reinforcement, owing to the excellent tensile properties of ECC materials. The average crack spacing and width decrease with the increase of ECC height replacement ratio. The ductility of hybrid reinforced composite beams is higher than that of traditional reinforced concrete beams while their practical reinforcement ratios are similar. Reinforced ECC beams show considerable energy dissipation capacity owing to ECC's excellent deformation ability. Considering the

23 constitutive models of materials, compatibility and equilibrium conditions, formulas for the  
24 prediction of cracking, yield and ultimate moments as well as deflections of hybrid reinforced  
25 ECC-concrete composite beams are developed. The proposed formulas are in good agreement with  
26 the experimental results. A comprehensive parametric analysis is, then, conducted to illustrate the  
27 effect of reinforcement, ECC and concrete properties on the moment capacity, curvature, ductility  
28 and energy dissipation of composite beams.

29 **Keywords:** ECC; concrete; composite beams; hybrid reinforcement; flexural behavior; steel bars;  
30 FRP bars.

## 31 **Introduction**

32 Many reinforced concrete structures, for example bridges, dams and off-shore structures, are  
33 exposed to de-icing salts, combinations of temperature, moisture and chlorides, causing corrosion of  
34 steel reinforcement. They, consequently, deteriorate and cannot meet the requirement of ultimate  
35 limit state and durability. Over the last four decades, FRP materials are increasingly used as a  
36 substitute to steel reinforcement in concrete structures (Masmoudi et al.1998; Grace et al. 1999;  
37 Pecce et al. 2000; Aiello et al. 2000; Gravina et al. 2008; Tu et al. 2009; Soric et al. 2010) for the  
38 advantages of high strength and anti-erosion properties. But FRP reinforcement has the properties of  
39 low elastic modulus and linear deformation until rupture, leading to large deflections, crack widths  
40 and brittle failure, which have been obstructing FRP structures from being widely used in civil  
41 engineering.

42 In order to enhance both ductility and durability of concrete structures, some researchers (Aiello  
43 et al. 2002; Leung et al. 2003; Qu et al. 2009; Lau et al.2010; Kara et al. 2015; Ge et al. 2015)  
44 proposed hybrid steel and FRP reinforcement, where FRP reinforcement is located at the corners of

45 concrete elements and steel bars are placed inside providing more corrosion protection. The excellent  
46 crack control ability and durability of ECC material has encouraged the use of ECC in the tensile  
47 zone around the longitudinal steel reinforcement (Maalej et al. 1995; Wang et al.2001; Yuan et al.  
48 2014). The results showed that the flexural capacity and deformation ability have slightly improved,  
49 but the crack width before yielding of steel reinforcement has significantly reduced to be just 20% of  
50 that in conventional reinforced concrete beams (Zhang et al. 2006; Xu et al. 2009; Xu et al. 2010;  
51 Zhang et al. 2010; Maalej et al.2012; Xu et al. 2013; Ge et al. 2018). On the other hand, ECC beams  
52 (Cai et al. 2017) and ECC-concrete composite beams (Maalej et al.2005; Yuan et al. 2013)  
53 reinforced with FRP bars were also studied to solve cracking and deflection problems associated  
54 with brittleness of FRP reinforced beams.

55 In this paper, a more effective system, combining ECC and concrete as the main body of  
56 structural beams reinforced with hybrid steel and FRP bars is proposed. A comprehensive  
57 experimental investigation of hybrid composite reinforced concrete beams having various ECC  
58 height replacement ratio and reinforcement index is conducted and presented in this paper. An  
59 analytical technique is proposed for predicting the cracking, yield and ultimate moments as well as  
60 the failure modes and deflection response throughout the loading. The technique is based on realistic  
61 constitutive models of materials, compatibility of strains and equilibrium of forces. A detailed  
62 parametric study is, then, carried out to establish the variation of flexural behavior of composite  
63 beams with the main influential parameters. Simplified equations are also proposed for the ultimate  
64 moments for each mode of failure.

## 65 **Experimental program**

### 66 *Test specimens design*

67 In total, thirty two beam specimens were tested to examine the behavior of the proposed hybrid  
68 reinforced composite concrete system as well as validating the developed analytical analysis  
69 presented later in this paper. The test specimens were divided into eight groups according to the  
70 amount and combination of steel and FRP reinforcement, while each group comprised of four  
71 specimens with different ECC height replacement ratio  $r_h$  (defined as the ECC thickness in tension  
72 zone  $h_e$  to effective height of cross-section  $h_0$ ,  $r_h = h_e / h_0$ ). Test specimen reinforcement and ECC  
73 height replacement ratio are shown in table 1 and schematic diagram of specimens is shown in figure  
74 1. In each group, four ECC height replacement ratio was selected, namely  $r_h = 0.00, 0.29, 0.57$  and  
75  $1.14$ , where  $r_h = 0.00$  and  $1.14$  indicate fully traditional concrete and fully ECC beam specimens,  
76 respectively. The cross-section width  $b$  and cross-section height  $h$  are 150 mm and 200 mm,  
77 respectively; specimen length  $l$ , pure flexural length  $l_m$ , flexural-shear length  $l_{mv}$  and free overhang  
78 length  $l_f$  are 1500 mm, 400 mm, 500 mm and 50 mm, respectively; cross-section effective height  $h_0$   
79 is 175 mm, the distance of the center of steel bars and the concrete tensile edge  $h_s$  is 25mm;  $A_s$  and  $A_f$   
80 are the cross-section areas of steel and FRP bars, respectively,  $\rho_s$  and  $\rho_f$  are the reinforcement ratio of  
81 steel and FRP bars ( $\rho_s = A_s / (bh_0)$ ,  $\rho_f = A_f / (bh_0)$ ), respectively,  $f_{tu}$  and  $f_y$  are the ultimate tensile  
82 strength of FRP bars and the yield strength of steel bars, respectively,  $E_f$  and  $E_s$  are the elastic  
83 modulus of FRP bars and steel bars, respectively,  $\rho_h (= \rho_s + \rho_f)$ ,  $\rho_{h,f} (= \rho_s + \rho_f f_{tu} / f_y)$  and  $\rho_{h,E} (= \rho_s +$   
84  $\rho_f E_f / E_s)$  represent the practical reinforcement ratio, nominal reinforcement ratio using strength  
85 conversion ratio ( $f_{tu} / f_y$ ) and nominal reinforcement ratio using elastic modulus conversion ratio ( $E_f /$   
86  $E_s$ ), respectively,  $A_{sv}$  and  $A_s'$  represent the stirrup and erection bars, respectively.

Table 1 Test specimen reinforcement and ECC height replacement ratio

Beam notation	$A_s$	$A_f$	$\rho_h$ (%)	$\rho_{h,f}$ (%)	$\rho_{h,E}$ (%)	$A_{sv}$	$A_s'$	$r_h$
HB	2 $\Phi$ 12	—	0.86	0.86	0.86	$\Phi$ 8@100	2 $\Phi$ 10	0.00/0.29/0.57/1.14
HC	2 $\Phi$ 12	$\Phi$ 8	1.05	1.56	0.91	$\Phi$ 8@100	2 $\Phi$ 10	0.00/0.29/0.57/1.14
HD	1 $\Phi$ 10	2 $\Phi$ 8	0.68	1.47	0.39	$\Phi$ 8@100	2 $\Phi$ 10	0.00/0.29/0.57/1.14
HE	1 $\Phi$ 12	2 $\Phi$ 8	0.81	1.60	0.53	$\Phi$ 8@100	2 $\Phi$ 10	0.00/0.29/0.57/1.14
HF	2 $\Phi$ 10	$\Phi$ 8	0.79	1.19	0.65	$\Phi$ 8@100	2 $\Phi$ 10	0.00/0.29/0.57/1.14
HG	2 $\Phi$ 12	$\Phi$ 8	1.05	1.45	0.91	$\Phi$ 8@100	2 $\Phi$ 10	0.00/0.29/0.57/1.14
HH	2 $\Phi$ 12	$\Phi$ 8	1.05	1.33	0.91	$\Phi$ 8@62.5	2 $\Phi$ 10	0.00/0.29/0.57/1.14
HK	—	3 $\Phi$ 8	0.57	1.76	0.14	$\Phi$ 8@100	2 $\Phi$ 10	0.00/0.29/0.57/1.14

88 Note:  $\Phi$ , HRB335 grade steel bar;  $\Phi$ , HRB400 grade steel bar;  $\Phi$ , HRB500 steel bar;  $\Phi$ , FRP bar.

89 Displacement transducers were used to measure the deflections at the support points, loading  
90 points and mid-span. Strain gauges were also arranged along the height of the beam cross-section to  
91 measure the strains in ECC/concrete. An oil hydraulic jack was used to load each specimen through a  
92 steel beam spreader to achieve the two point loading system shown in figure 1.

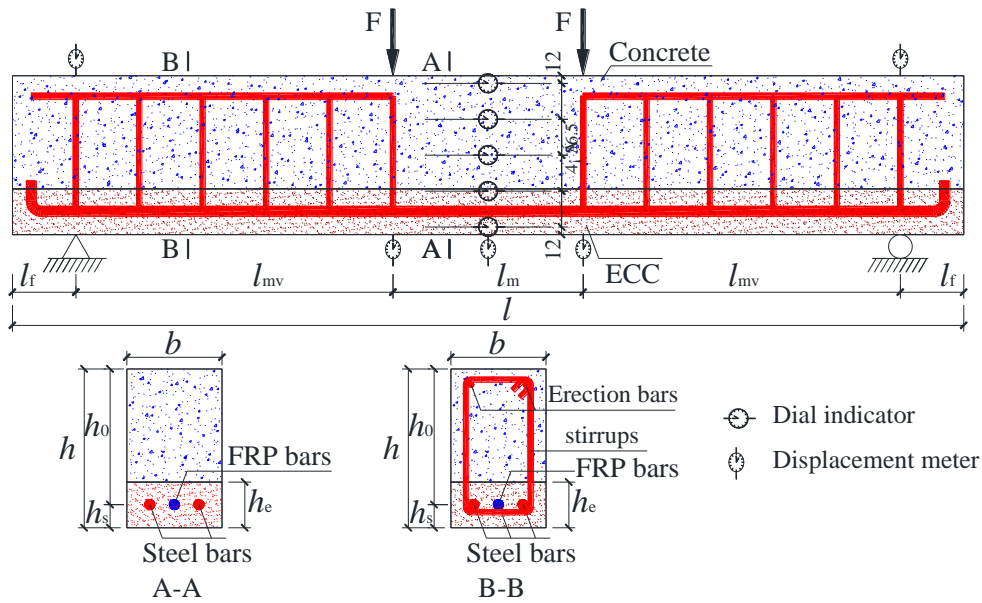


Fig.1 Schematic diagram of hybrid reinforced ECC-concrete composite beams

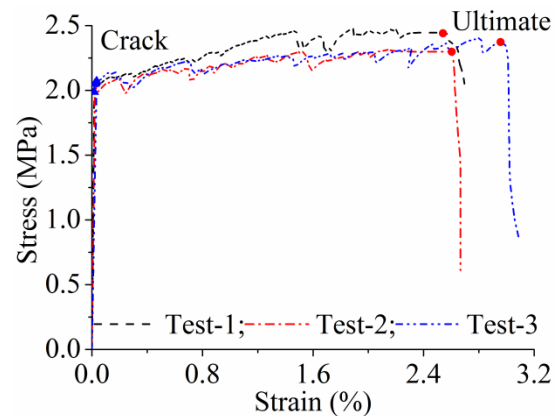
### 93 **Materials**

94 Portland cement, grade I fly ash, superfine silica fume, 100-200 mesh special fine quartz sand,  
95 sika poly acid water reducer and RECS15\*12 type polyvinyl alcohol (PVA) fiber were used for

96 producing ECC. The mass ratio of cement, fly ash, silica fume, sand and water were 1.0 : 3.0 : 1.0 :  
 97 0.36 : 0.3, and the fiber volume fraction is 2.0 %. Figure 2 presents the tensile stress-strain curves of  
 98 ECC used, obtained from testing three rectangular flat-plates with a size of 160 mm × 40 mm × 15  
 99 mm in tension. The tensile stress at first cracking  $f_{etc} = 2.0$  MPa, ultimate tensile strength  $f_{tu} = 2.4$   
 100 MPa, tensile elastic modulus  $E_e = 8.2$  GPa, tensile strain at first cracking  $\varepsilon_{etc} = 0.23 \times 10^{-3}$  and  
 101 ultimate tensile strain  $\varepsilon_{etu} = 0.025$ . On the other hand, three prismatic specimens with a size of 40  
 102 mm × 40 mm × 160mm were made for compressive tests and the compressive stress-strain of ECC  
 103 are shown in figure 3. The peak compressive stress of ECC  $f_{ecp} = 31.4$  MPa and its corresponding  
 104 strain  $\varepsilon_{ecp} = 0.0036$ .



(a) Test

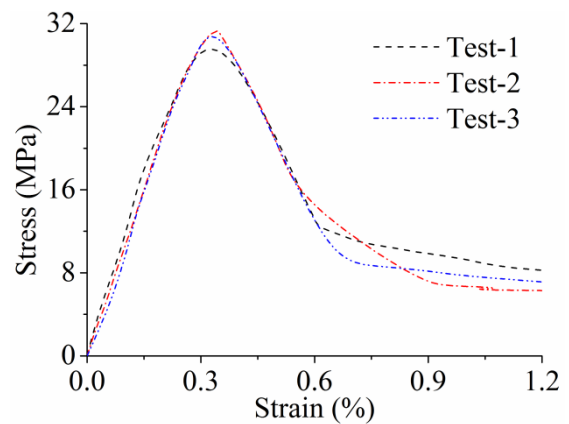


(b) Stress-strain curves

Fig.2 Tensile test of ECC



(a) Test



(b) Stress-strain curves

Fig.3 Compressive test of ECC

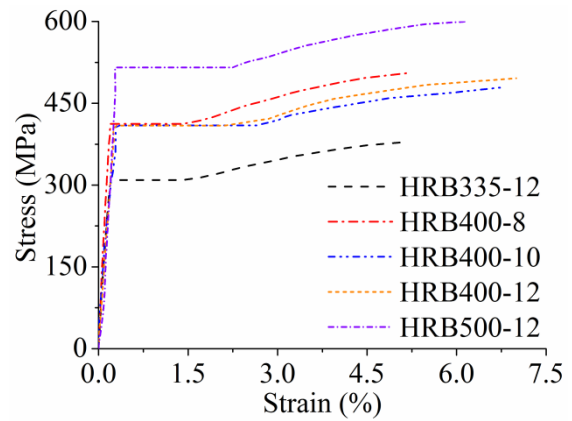
105 The mechanical properties of steel bars were measured as listed in table 2 and figure 4, where  $f_y$ ,  
 106  $f_u$  and  $E$  are the yield strength, ultimate strength and elastic modulus of reinforcing steel bars,  
 107 respectively.

Table 2 Mechanical properties of reinforcing bars

Bar type	Diameter (mm)	$f_y$ (MPa)	$f_u$ (MPa)	$E$ (GPa)
HRB335	12	340	460	199
HRB400	8	406	485	198
HRB400	10	403	495	198
HRB400	12	408	503	199
HRB500	12	507	630	199
BFRP	8	—	1250	50



(a) Test



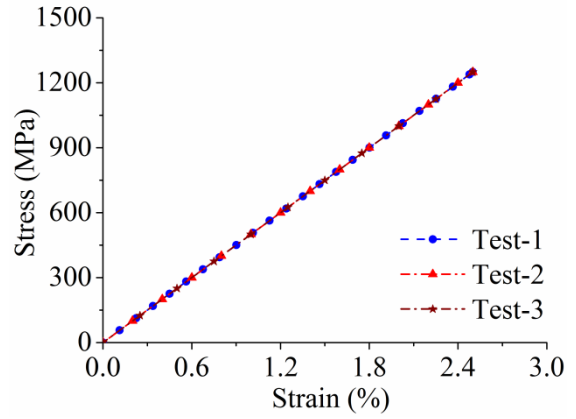
(b) Stress-strain curves

Fig.4 Tensile test of steel reinforcement

109 The mechanical properties of basalt fiber reinforced polymer (BFRP) bars was obtained from  
 110 testing three specimens according to ACI 440.3R-04(ACI 2004) as shown in figure 5(a); the total  
 111 length of the specimen was 1200 mm and the free length was 400 mm. The stress-strain curves are  
 112 shown in figure 5(b) and its tensile prosperities are shown in table 2.



(a) Test



(b) Stress-strain curves

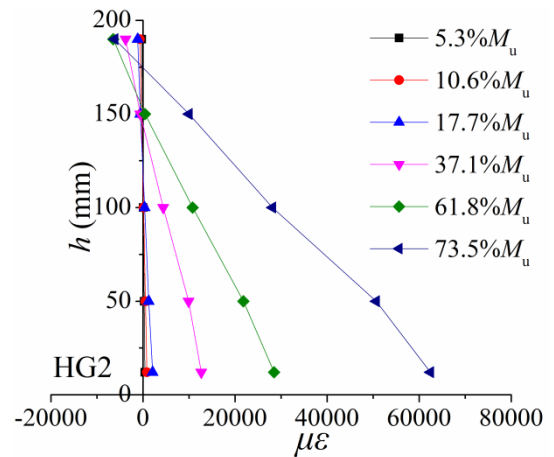
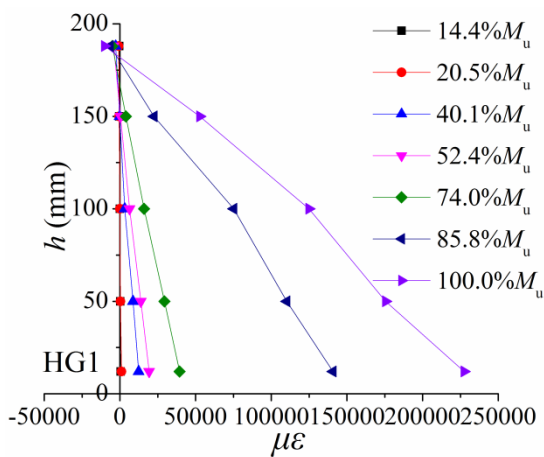
Fig.5 Tensile test of FRP rebar

113 Three cube specimens with a size of 150 mm × 150 mm × 150mm were made for concrete  
 114 mechanical properties tests (Chinese National Standard 2002; Chinese National Standard 2010).  
 115 Compressive strength  $f_c = 30.16$  MPa, tensile strength  $f_t = 2.55$  MPa and ultimate tensile strain  $\epsilon_{tu} =$   
 116  $110 \times 10^{-6}$ .

117 **Experimental results**

118 *Strain distribution along the height of cross-section*

119 Average ECC/concrete strain distributions along the height of cross-section (group HG) for  
 120 various acting moments are shown in figure 6. Other groups exhibited similar strain distribution,  
 121 therefore not presented here.



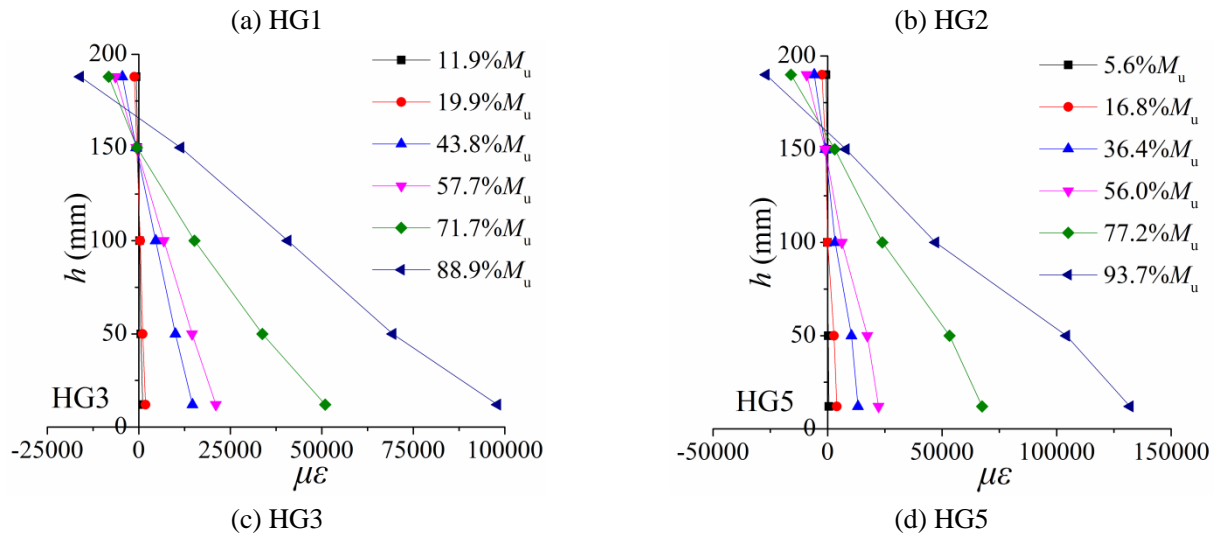


Fig.6 Average strain distribution along the height of cross-section

122 Figure 6 shows that the strain distribution is almost linear, indicating that:

- 123 • The validity of the assumption that plane section perpendicular to the axis of the beam
- 124 remains plane after loading;
- 125 • No delamination between ECC and concrete at various stages of loading in this
- 126 investigation.

### 127 ***Loading-deflection curves***

128 For the hybrid reinforced ECC beams, tiny cracks were first observed in the pure bending

129 region as the load increased. After that, the slope of the load-deflection curve showed a slight drop

130 and new flexural cracks were formed in the beam with the increase of loading. For beams having

131 steel reinforcement, yielding of such reinforcement was reached, followed by a quick increase in the

132 mid-span deflection and crack width with little increase of the applied load. With further increase of

133 loading, the outermost fiber of concrete in the compression zone reached the ultimate strain and

134 crushed, indicating a compressive failure mode. The crack patterns and failure modes at failure of

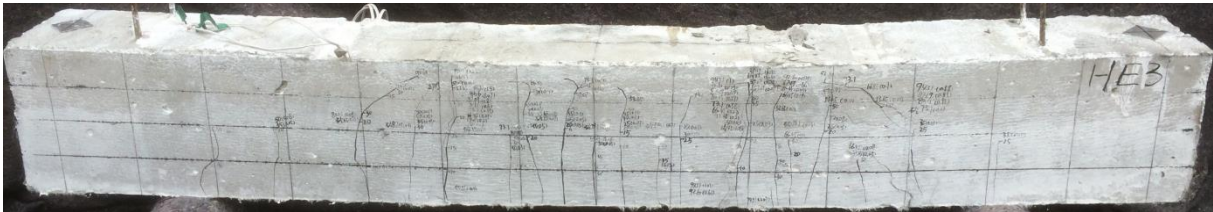
135 specimens HE1, HE2, HE3 and HE5 are shown in figure 7.



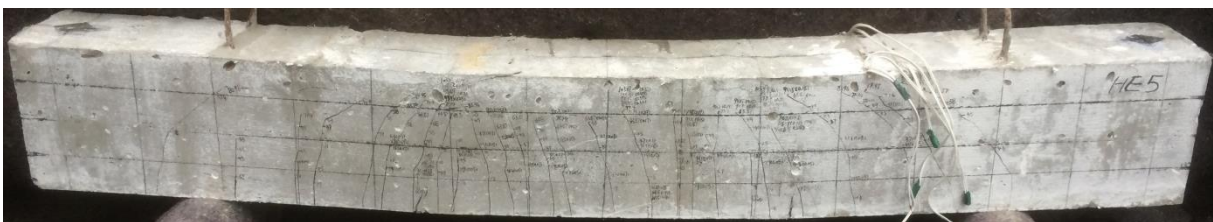
(a) HE1



(b) HE2



(c) HE3



(d) HE5

Fig.7 Crack patterns and failure modes of group HE

136 The mid-span moment-deflection ( $M-f$ ) curves of groups HB, HE, HF and HK are shown in  
137 figure 8. The mid-span deflection  $f$  can be obtained by subtracting the average settlement value of the  
138 two bearing points with the measured deformation of mid-span, whereas the moment  $M$  can be  
139 obtained by multiplying the measured load  $F$  by flexural-shear length  $l_{mv}$  (as shown in figure 1).

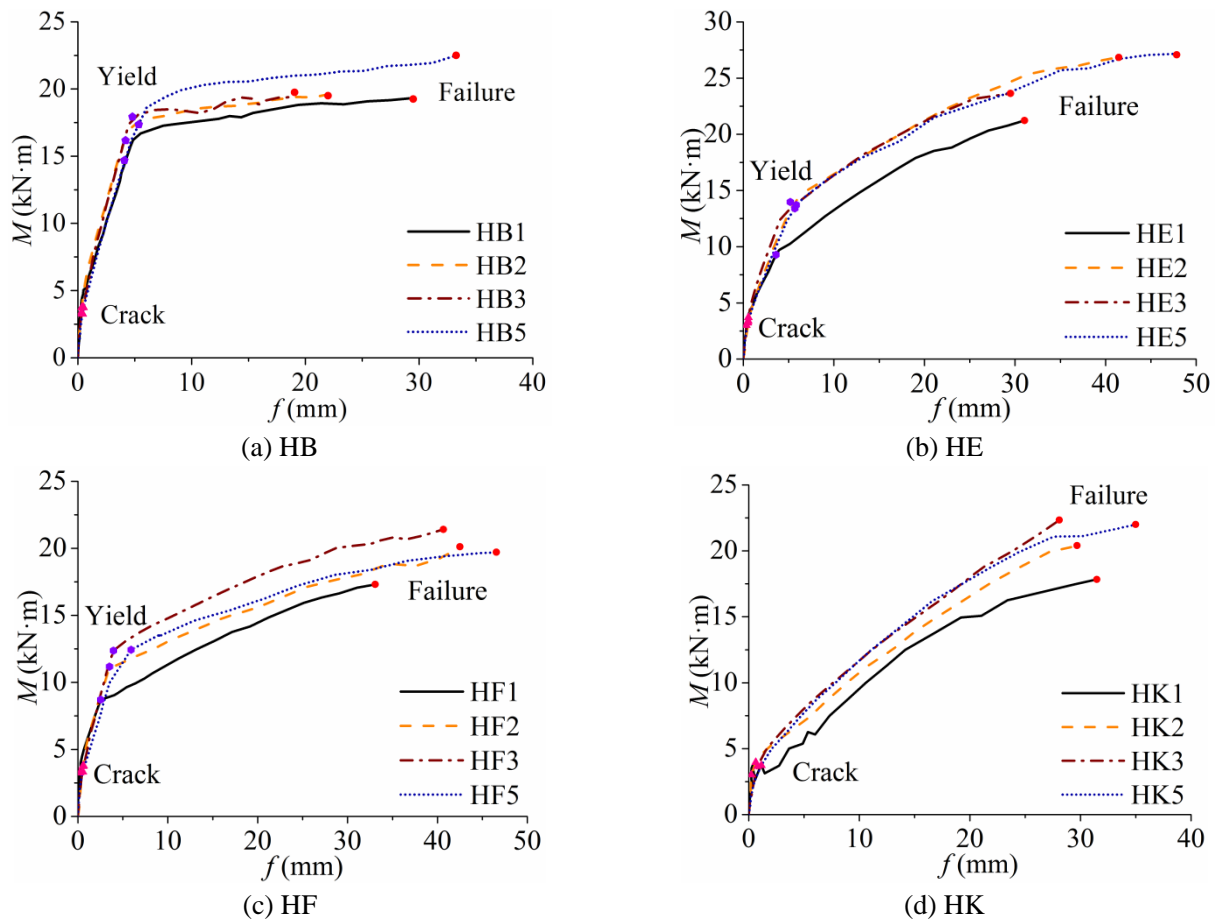


Fig.8 Comparison of moment-deflection curves

140 As can be observed from figures 7 and 8, no delamination between concrete and ECC layer was  
 141 detected until failure. At the same applied load, the deflection of composite beams and ECC beams  
 142 are less than that of concrete beams, regardless of the reinforcement used, indicating that higher  
 143 stiffness can be obtained when ECC is used. The loading process of steel reinforced beams and  
 144 hybrid reinforced beams can be divided into three stages: 1). from being loaded to the cracking of  
 145 concrete/ECC; 2). from cracking to yielding of steel reinforcement and 3) from yielding of steel  
 146 reinforcement to failure. After yielding of steel bars, the deflections of the steel reinforced beams  
 147 continually increased even the load does not increase while deflections of hybrid reinforced beams  
 148 increased with the increase of loading. On the other hand, the loading process of FRP reinforced  
 149 beams can be divided into two stages: 1). from being loaded to the cracking of concrete/ECC and 2).

150 from cracking to failure of beams.

151 ***Cracking, yield and ultimate moment***

152 Cracking, yield, ultimate moments and corresponding deflections of specimens are shown in  
 153 table 3.

154 Table 3 Experimental values of cracking, yield and ultimate moments and corresponding deflections

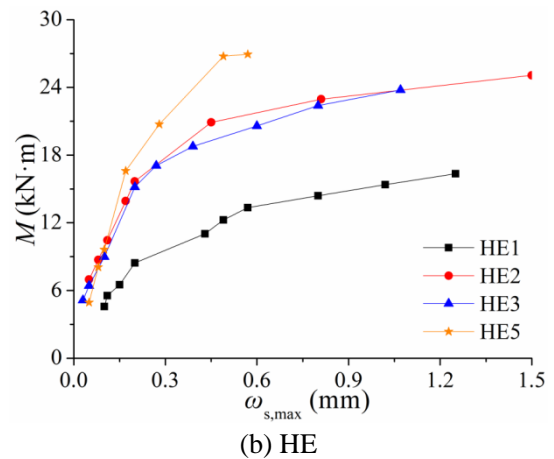
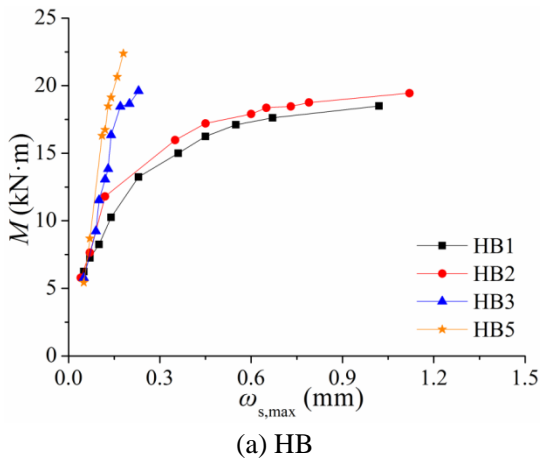
Beam notation	$\rho_h$ (%)	$\rho_{h,f}$ (%)	$\rho_{h,E}$ (%)	$r_h$	$M_{cr,e}$ (kN·m)	$d_{cr,e}$ (mm)	$M_{y,e}$ (kN·m)	$d_{y,e}$ (mm)	$M_{u,e}$ (kN·m)	$d_{u,e}$ (mm)
HB1				0.00	3.26	0.25	14.7	4.09	19.3	29.5
HB2	0.86	0.86	0.86	0.29	3.74	0.34	16.2	4.20	19.5	22.0
HB3				0.57	3.75	0.48	17.9	4.80	19.8	19.1
HB5				1.14	3.26	0.41	17.4	5.36	22.5	33.3
HC1				0.00	3.26	0.23	14.0	2.92	22.0	29.5
HC2	1.05	1.56	0.91	0.29	4.00	0.27	17.4	4.12	23.9	33.8
HC3				0.57	3.74	0.50	19.6	4.92	25.7	32.8
HC5				1.14	3.56	0.68	16.9	5.29	24.8	39.1
HD1				0.00	3.00	0.13	7.02	3.69	18.3	31.4
HD2	0.68	1.47	0.39	0.29	3.26	0.34	9.45	4.38	18.6	30.6
HD3				0.57	3.25	0.45	10.7	4.59	22.0	29.1
HD5				1.14	3.00	0.72	10.7	6.48	21.9	51.0
HE1				0.00	3.02	0.32	9.28	3.62	21.2	31.1
HE2	0.81	1.60	0.53	0.29	3.39	0.54	14.0	5.19	26.8	41.5
HE3				0.57	3.71	0.56	13.4	5.70	23.6	29.5
HE5				1.14	3.23	0.50	13.7	5.85	27.1	47.9
HF1				0.00	3.26	0.22	8.71	2.53	17.3	33.1
HF2	0.79	1.19	0.65	0.29	3.75	0.56	11.2	3.52	20.1	42.5
HF3				0.57	3.77	0.64	12.4	3.96	21.4	40.7
HF5				1.14	3.33	0.55	12.4	5.91	19.7	46.6
HG1				0.00	3.46	0.20	17.3	4.14	24.3	31.4
HG2	1.05	1.45	0.91	0.29	3.82	0.26	17.5	4.70	28.3	30.3
HG3				0.57	3.80	0.29	18.8	6.11	25.1	28.5
HG5				1.14	3.55	0.50	18.4	6.15	26.8	43.9
HH1				0.00	3.49	0.27	19.5	4.32	26.6	24.2
HH2	1.05	1.33	0.91	0.29	3.75	0.36	23.2	5.17	28.8	27.3
HH3				0.57	3.99	0.37	23.9	5.29	28.7	23.8
HH5				1.14	3.59	0.51	23.7	7.63	27.2	38.3
HK1				0.00	3.02	0.23	—	—	17.8	31.5
HK2	0.57	1.76	0.14	0.29	3.97	0.63	—	—	20.4	29.7
HK3				0.57	3.66	0.79	—	—	22.3	28.1
HK5				1.14	3.73	1.15	—	—	22.0	35.0

155 Note:  $M_{cr,e}$ ,  $M_{y,e}$  and  $M_{u,e}$  are the experimental cracking, yield and ultimate moment, respectively,  $d_{cr,e}$ ,  $d_{y,e}$  and  $d_{u,e}$   
 156 are the corresponding deflection of cracking, yield and ultimate moment, respectively.

157 As can be observed from table 3, the cracking, yield and ultimate moments of composite beams  
 158 and ECC beams are higher than those of concrete beams, regardless of the reinforcement used. For  
 159 specimens with the same nominal reinforcement ratio using elastic modulus conversion factor  
 160 ( $\rho_{h,E,HC} = \rho_{h,E,HG} = \rho_{h,E,HH} = 0.91\%$ ), ultimate moment increases with the decrease of nominal  
 161 reinforcement ratio using strength conversion factor ( $\rho_{h,f,HC} = 1.38\% > \rho_{h,f,HG} = 1.34\% > \rho_{h,f,HH} =$   
 162  $1.24\%$ ). For specimens with similar nominal reinforcement ratio converted by strength ratio ( $\rho_{h,f,HC}$   
 163  $= 1.56\% \approx \rho_{h,f,HE} = 1.60\%$ ,  $\rho_{h,f,HD} = 1.47\% \approx \rho_{h,f,HG} = 1.45\%$ ), yield moment decreases with the  
 164 decrease of nominal reinforcement ratio converted by elastic modulus ratio ( $\rho_{h,E,HC} = 0.91\% > \rho_{h,E,HE}$   
 165  $= 0.53\%$ ,  $\rho_{h,E,HG} = 0.91\% > \rho_{h,E,HD} = 0.39\%$ ).

166 ***Cracks distribution and Failure mode***

167 The moment-crack width ( $M-\omega_{s,max}$ ) curves, number of cracks ( $n$ ) and average crack spacing ( $l_{cr}$ )  
 168 of groups HB, HE, HF and HK are shown in figure 9 and figure 10, respectively.



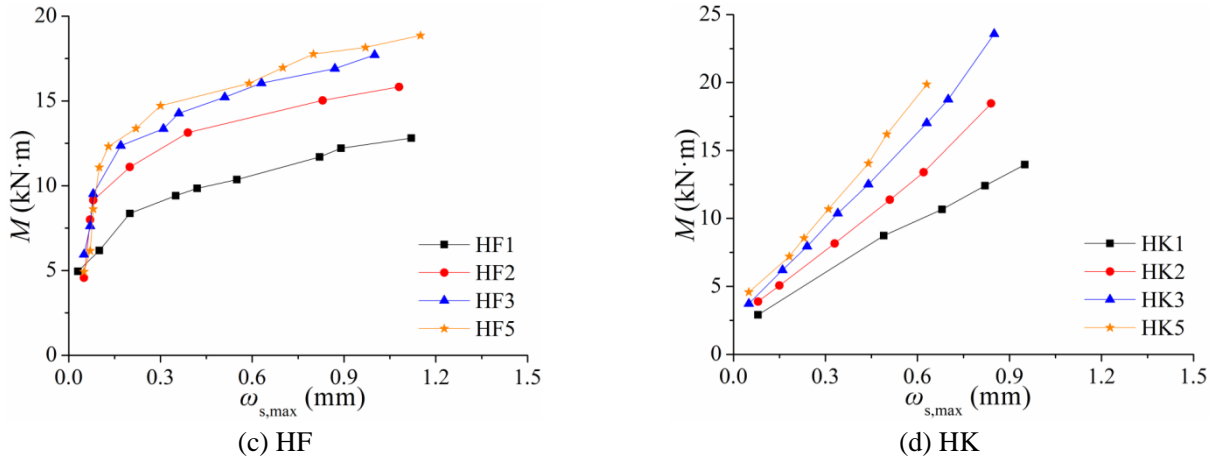


Fig.9 Comparison of load-crack width curves

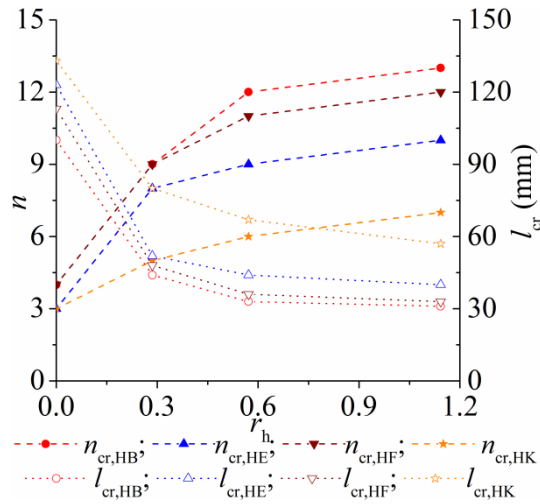


Fig.10 Number of cracks and average crack spacing of groups HB, HE, HF and HK

169 As can be observed from figures 9 and 10, number of cracks increases while average crack  
 170 spacing decreases with the increase of height replacement ratio. According to the experimental  
 171 observation, the maximum crack width of specimens decrease with increasing the height replacement  
 172 ratio, regardless of the reinforcement used. Taking group HF as example, under the same moment of  
 173 12.0 kN·m, the maximum crack width of specimens HF1, HF2, HF3 and HF5 are 0.86 mm, 0.28 mm,  
 174 0.16 mm and 0.12 mm, respectively.

### 175 ***Ductility and energy dissipation***

176 Ductility and energy dissipation of specimens are shown in table 4,  $u_d$  is the deflection ductility  
 177 defined as the ultimate deflection  $d_u$  to yield deflection  $d_y$ ,  $u_d = d_u / d_y$ ,  $E_d$  is the energy dissipation (in

178  $\text{N}\cdot\text{m}^2$ ) defined by the including area of the moment-deflection ( $M-d$ ) curves, for steel reinforced  
179 beams and hybrid reinforced beams,  $E_d = M_{cr} d_{cr} / 2 + (M_{cr} + M_y) (d_y - d_{cr}) / 2 + (M_y + M_u) (d_u - d_y)$   
180  $/ 2$ , for FRP reinforced beams,  $E_d = M_{cr} d_{cr} / 2 + (M_{cr} + M_u) (d_u - d_{cr}) / 2$ .

181 Table 4 Ductility and energy dissipation of specimens

Beam notation	$\rho_h$ (%)	$\rho_{h,f}$ (%)	$\rho_{h,E}$ (%)	$r_h$	$u_d$	$E_d$ ( $\text{N}\cdot\text{m}^2$ )
HB1				0.00	7.21	466
HB2				0.29	5.24	357
HB3	0.86	0.86	0.86	0.57	3.97	316
HB5				1.14	6.21	608
HC1				0.00	10.1	502
HC2				0.29	8.21	655
HC3	1.05	1.56	0.91	0.57	6.66	684
HC5				1.14	7.38	752
HD1				0.00	8.50	369
HD2				0.29	6.99	395
HD3	0.68	1.47	0.39	0.57	6.33	429
HD5				1.14	7.87	767
HE1				0.00	8.58	439
HE2				0.29	7.99	781
HE3	0.81	1.60	0.53	0.57	5.18	486
HE5				1.14	8.18	903
HF1				0.00	13.1	412
HF2				0.29	12.1	633
HF3	0.79	1.19	0.65	0.57	10.3	648
HF5				1.14	7.87	696
HG1				0.00	7.58	608
HG2				0.29	6.46	635
HG3	1.05	1.45	0.91	0.57	4.66	558
HG5				1.14	7.14	917
HH1				0.00	5.61	507
HH2				0.29	5.27	641
HH3	1.05	1.33	0.91	0.57	4.50	556
HH5				1.14	5.03	880
HK1				0.00	—	326
HK2				0.29	—	355
HK3	0.57	1.76	0.14	0.57	—	356
HK5				1.14	—	438

182 As can be observed from table 4, the ductility of composite beams is less than that of concrete

183 beams as ECC can provide tensile stress until failure, but the energy dissipation of reinforced ECC  
 184 beams is higher than that of reinforced concrete beams and composite beams as the ultimate  
 185 compressive strain of ECC is higher than that of concrete. For composite beams, ductility decreases  
 186 with the increase of ECC height replacement ratio. For specimens with similar practical  
 187 reinforcement ratio ( $\rho_{h,HB} = 0.86 \% \approx \rho_{h,HE} = 0.81 \%$ ), ductility of hybrid reinforced beams are higher  
 188 than that of reinforced concrete beams. For specimens with the same nominal reinforcement ratio  
 189 converted by elastic modulus ( $\rho_{h,E,HC} = \rho_{h,E,HG} = \rho_{h,E,HH} = 0.91 \%$ ), ductility increases with the  
 190 increase of nominal reinforcement ratio converted by strength. Energy dissipation of steel reinforced  
 191 beams and hybrid reinforced beams are higher than that of FRP reinforced beams.

192 **Materials constitutive model**

193 ***Reinforcement***

194 The constitutive relationships of steel bars and FRP bars are shown in figure 11, where  $\sigma$  and  $\varepsilon$   
 195 are the stress and strain in materials, respectively;  $f_{sy}$ ,  $E_s$ ,  $\varepsilon_{sy}$  and  $\varepsilon_{su}$  are the yield strength, elastic  
 196 modulus, yield strain and ultimate tensile strain (assumed to be 0.01) of steel bars, respectively;  $f_{fu}$ ,  
 197  $E_f$  and  $\varepsilon_{fu}$  are the tensile strength, elastic modulus and ultimate tensile strain of FRP bars,  
 198 respectively.

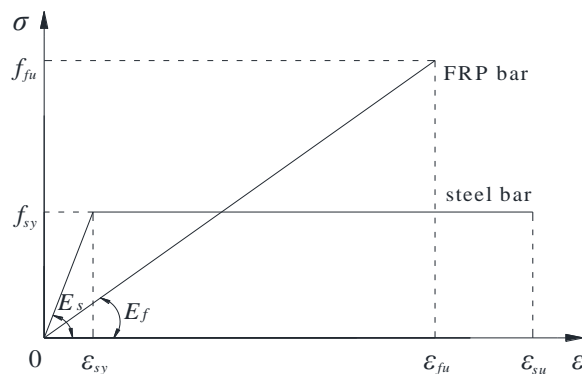


Fig.11 Constitutive relationships of steel bar

199 **Concrete**

200 The compressive stress-strain curve of concrete (Chinese National Standard 2010) is shown in  
 201 figure 12(a) and can be expressed by:

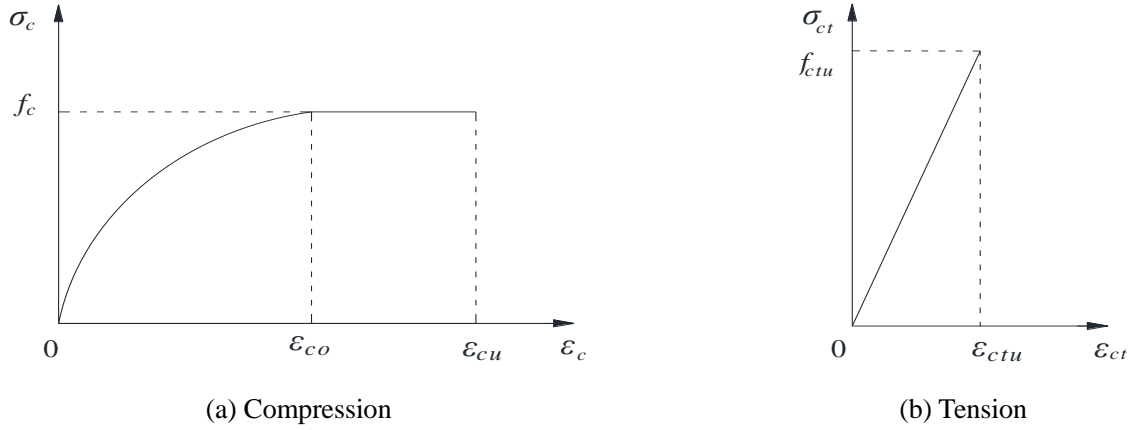


Fig.12 Constitutive relationships of concrete

$$\sigma_c = \begin{cases} f_c \left[ 1 - \left( 1 - \varepsilon_c / \varepsilon_{co} \right)^n \right] & , 0 \leq \varepsilon_c \leq \varepsilon_{co} \\ f_c & , \varepsilon_{co} < \varepsilon_c \leq \varepsilon_{cu} \end{cases} \quad (1)$$

$$n = 2 - (f_{cu,k} - 50) / 60 \quad (2)$$

$$\varepsilon_{co} = 0.002 + 0.5 (f_{cu,k} - 50) \times 10^{-5} \quad (3)$$

$$\varepsilon_{cu} = 0.0033 - 0.5 (f_{cu,k} - 50) \times 10^{-5} \quad (4)$$

202 where  $\varepsilon_c$  and  $\sigma_c$  are the compressive strain and stress in concrete,  $f_c$  is the concrete compressive  
 203 strength (in MPa),  $\varepsilon_{co}$  ( $\geq 0.002$ ) is the compressive strain corresponding to concrete stress of  $f_c$ ,  $\varepsilon_{cu}$  ( $\leq$   
 204 0.0033) is the ultimate compressive strain of concrete,  $f_{cu,k}$  is the concrete cube compressive strength  
 205 (in MPa) and  $n$  is a coefficient related to compressive strength of concrete ( $\leq 2.0$ ).

206 The concrete uniaxial tensile stress-strain model is shown in figure 12(b) and can be represented  
 207 by the following equation,

$$\sigma_{ct} = \begin{cases} f_{ctu} \varepsilon_{ct} / \varepsilon_{ctu} & , 0 \leq \varepsilon_{ct} \leq \varepsilon_{ctu} \\ 0 & , \varepsilon_{ct} > \varepsilon_{ctu} \end{cases} \quad (5)$$

208 where  $\varepsilon_{ct}$  and  $\sigma_{ct}$  are the tensile strain and stress in concrete,  $f_{ctu}$  and  $\varepsilon_{ctu}$  are the ultimate uniaxial  
 209 tensile stress and corresponding strain.

### 210 ECC

211 The compressive stress-strain curve (Yuan et al. 2013) of ECC is shown in figure 13(a) and can  
 212 be formulated by:

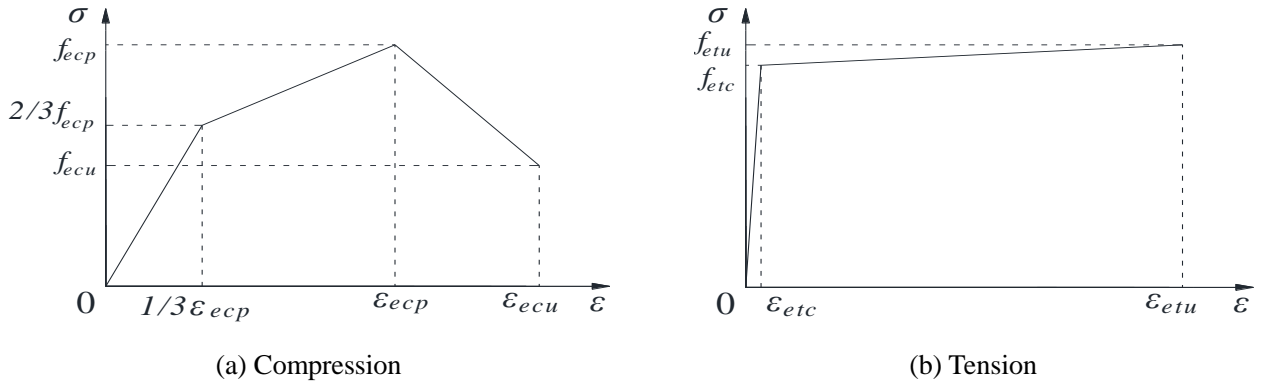


Fig.13 Constitutive relationships of ECC

$$\sigma_{ec} = \begin{cases} 2f_{ecp} \varepsilon_{ec} / \varepsilon_{ecp} & , 0 \leq \varepsilon_{ec} \leq \varepsilon_{ecp} / 3 \\ f_{ecp} / 2 + f_{ecp} \varepsilon_{ec} / (2\varepsilon_{ecp}) & , \varepsilon_{ecp} / 3 < \varepsilon_{ec} \leq \varepsilon_{ecp} \\ 2f_{ecp} - f_{ecp} \varepsilon_{ec} / \varepsilon_{ecp} & , \varepsilon_{ecp} < \varepsilon_{ec} \leq \varepsilon_{ecu} \end{cases} \quad (6)$$

213 where  $\varepsilon_{ec}$  and  $\sigma_{ec}$  are the compressive strain and stress in ECC,  $f_{ecp}$  is the compressive strength of  
 214 ECC (peak point of the curve),  $\varepsilon_{ecp}$  is the compressive strain corresponding to peak stress  $f_{ecp}$ ,  $f_{ecu}$  is  
 215 the ultimate compressive stress (after peak point) and  $\varepsilon_{ecu}$  is the ultimate compressive strain  
 216 corresponding to ultimate stress  $f_{ecu}$ . In this paper, it is assumed that  $f_{ecu} = 0.5 f_{ecp}$  and  $\varepsilon_{ecu} = 1.5 \varepsilon_{ecp}$   
 217 (Yuan et al. 2013).

218 The tensile stress-strain curve (Maalej et al. 1995) of ECC is shown in figure 13(b) and can be  
 219 expressed by the following equation,

$$\sigma_{et} = \begin{cases} f_{etc} \varepsilon_{et} / \varepsilon_{etc} & , 0 \leq \varepsilon_{et} \leq \varepsilon_{etc} \\ f_{etc} + (f_{etu} - f_{etc}) (\varepsilon_{et} - \varepsilon_{etc}) / (\varepsilon_{etu} - \varepsilon_{etc}) & , \varepsilon_{etc} < \varepsilon_{et} \leq \varepsilon_{etu} \end{cases} \quad (7)$$

220 where  $\varepsilon_{et}$  and  $\sigma_{et}$  are the tensile strain and stress in ECC,  $f_{etc}$  and  $\varepsilon_{etc}$  are the tensile strength and  
 221 corresponding strain at first cracking,  $f_{etu}$  and  $\varepsilon_{etu}$  are the ultimate tensile strength and corresponding  
 222 strain.

## 223 Cracking and failure mode

### 224 Cracking modes

225 The cross-section strain distribution of ECC-concrete beams is shown in figure 14, where  $b$  is  
 226 the width of cross-section,  $h$  is the height of cross-section,  $h_s$  is the distance of the core of steel/FRP  
 227 bars to the cross-section tensile edge,  $h_e$  is the thickness of ECC,  $h_t$  is the height of cross-section part  
 228 in tension (neutral axis depth),  $\varepsilon_{et}$  is the maximum tensile strain in ECC,  $\varepsilon_{ct}$  is the maximum tensile  
 229 strain in concrete,  $\varepsilon_c$  is the maximum compressive strain in concrete,  $\varepsilon_s$  and  $\varepsilon_f$  are the tensile strain in  
 230 steel and FRP bars, respectively.

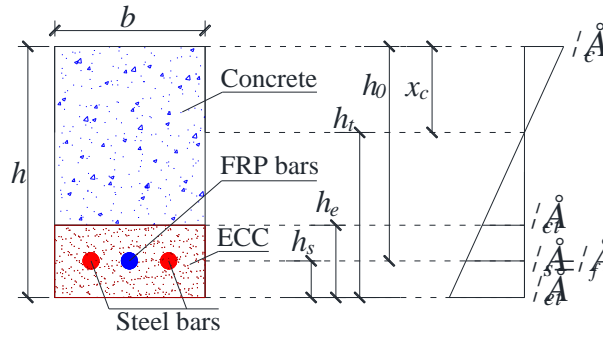


Fig.14 Cross-section strain distribution of elastic stage

231 If ECC and concrete simultaneously crack, the maximum ECC tensile strain  $\varepsilon_{et} = \varepsilon_{etc}$  and  
 232 maximum concrete tensile strain  $\varepsilon_{ct} = \varepsilon_{ctu}$ . According to the geometric similarity relationship, the  
 233 following equation can be obtained,

$$\varepsilon_{ctu} / \varepsilon_{etc} = (h_t - h_{e,b}) / h_t \quad (8)$$

234 where  $h_{e,b}$  is the thickness of ECC that makes ECC and concrete incur cracking at the same time.

235 And then, the balance ECC thickness  $h_{e,b}$  can be expressed as below:

$$h_{e,b} = (1 - \varepsilon_{ctu} / \varepsilon_{etc}) h_t \quad (9)$$

236 If  $h_e < h_{e,b}$ , concrete cracks before ECC, and when  $h_e > h_{e,b}$ , ECC incurs crack before concrete.

237 **Failure Modes**

238 According to the constitutive models of materials, failure modes of hybrid composite beams can  
 239 be divided into three situations. The boundary state of failure modes is shown in figure 15, where  $\varepsilon_{hu}$   
 240 is the minimum ultimate tensile strain of steel and FRP bars,  $\varepsilon_{hu} = \min(\varepsilon_{su}, \varepsilon_{fu})$ ,  $x_c$  is the height of  
 241 compressive zone.

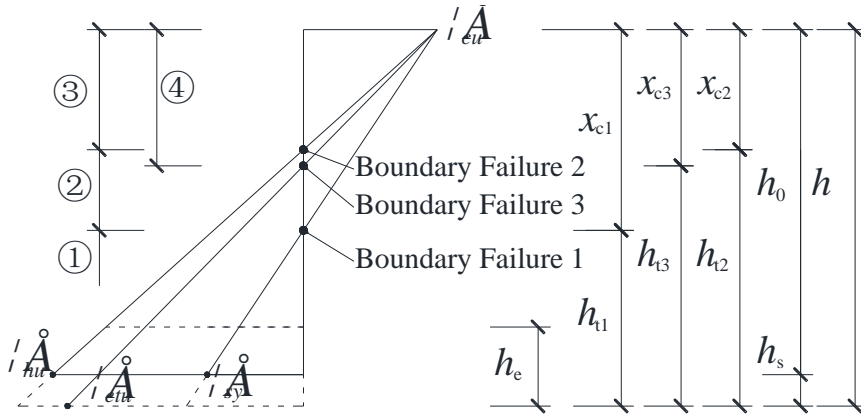


Fig.15 Cross-section strain distribution of boundary state

242 ①  $\varepsilon_c = \varepsilon_{cu}, \varepsilon_s = \varepsilon_f < \varepsilon_{sy}$

243 In this case, the steel bars do not yield, but the maximum compressive strain reaches the  
 244 ultimate strain of concrete. This situation is similar to over-reinforced concrete beams and is not  
 245 allowed in practical situations for its brittle failure.

246 ②  $\varepsilon_c = \varepsilon_{cu}, \varepsilon_{sy} < \varepsilon_s = \varepsilon_f \leq \varepsilon_{hu}$

247 The steel bars have yielded but its strain value does not reach the ultimate tensile strain of steel  
 248 bars and FRP bars. However, the failure occurs when the concrete compressive strain reaches its

249 ultimate strain. This situation is expected in practical structures for its ductile nature.

250 ③  $\varepsilon_c < \varepsilon_{cu}, \varepsilon_{sy} < \varepsilon_s = \varepsilon_f = \varepsilon_{hu}$

251 The steel bars have yielded and its strain value reaches the ultimate tensile strain of steel bars  
252 and FRP bars. On the other hand, the compressive concrete strain does not reach the ultimate  
253 concrete compressive strain. This situation is not practically allowed as the amount of steel  
254 reinforcement is very small, allowing very large strains in steel.

255 ④  $\varepsilon_c < \varepsilon_{cu}, \varepsilon_{sy} < \varepsilon_s = \varepsilon_f < \varepsilon_{hu}, \varepsilon_{et} = \varepsilon_{etu}$

256 The steel bars have yielded but its strain value does not reach the ultimate tensile strain of steel  
257 bars and FRP bars and the compressive concrete strain does not reach the ultimate concrete  
258 compressive strain. However, the failure occurs when the ECC tensile strain reaches its ultimate  
259 strain.

260 According to the force equilibrium of cross-section, the following equation can be obtained,

$$\int_0^{x_c} \sigma_c b dx = \sigma_s A_s + \sigma_f A_f + \int_0^{h_c} \sigma_{et} b dx \quad (10)$$

261 where  $x_c$  is the height of the compressive zone,  $x_c = \varepsilon_{cu} h_0 / (\varepsilon_{cu} + \varepsilon_s)$ .

262 Assuming the relative boundary compressive height  $\xi_c = x_c / h_0$ . The boundary relative neutral  
263 axis height  $\xi_{cb}$  can be defined according to the plane section assumption.

264 Boundary Failure 1:

$$\xi_{cb1} = \frac{x_{c1}}{h_0} = \frac{\varepsilon_{cu}}{\varepsilon_{cu} + \varepsilon_{sy}} \quad (11)$$

265 Boundary Failure 2:

$$\xi_{cb2} = \frac{x_{c2}}{h_0} = \frac{\varepsilon_{cu}}{\varepsilon_{cu} + \varepsilon_{hu}} \quad (12)$$

266 Boundary Failure 3:

$$\xi_{cb3} = \frac{x_{c3}}{h_0} = \frac{\varepsilon_{cu}}{\varepsilon_{cu} + \varepsilon_{ctu}} \quad (13)$$

267 For concrete grade less than C50 and considering tensile stress in ECC  $\sigma_{et} = f_{etc}$  and  $r_h = h_c / h_0$ ,

268 Eq. (12) can be modified as below:

$$f_c b h_0 \frac{\varepsilon_{cu} - \varepsilon_{co}/3}{\varepsilon_{cu} + \varepsilon_s} = \sigma_s A_s + \sigma_f A_f + f_{etc} b h_e \quad (14)$$

269 For Boundary Failure 1,

$$\rho_s + \frac{E_f}{E_s} \rho_f = \frac{f_c}{f_y} \cdot \frac{\varepsilon_{cu} - \varepsilon_{co}/3}{\varepsilon_{cu} + \varepsilon_{sy}} - r_h \frac{f_{etc}}{f_y} \quad (15)$$

270 For Boundary Failure 2,

$$\text{If } \varepsilon_{su} < \varepsilon_{fu}, \quad \rho_s + \frac{E_f}{E_s} \cdot \frac{\varepsilon_{su}}{\varepsilon_{sy}} \rho_f = \frac{f_c}{f_y} \cdot \frac{\varepsilon_{cu} - \varepsilon_{co}/3}{\varepsilon_{cu} + \varepsilon_{su}} - r_h \frac{f_{etc}}{f_y} \quad (16)$$

$$\text{If } \varepsilon_{su} \geq \varepsilon_{fu}, \quad \rho_s + \frac{f_{fu}}{f_y} \rho_f = \frac{f_c}{f_y} \cdot \frac{\varepsilon_{cu} - \varepsilon_{co}/3}{\varepsilon_{cu} + \varepsilon_{fu}} - r_h \frac{f_{etc}}{f_y} \quad (17)$$

271 For Boundary Failure 3,

$$\rho_s + \frac{E_f}{f_y} \cdot \frac{h_0 \varepsilon_{etu} - h_s \varepsilon_{cu}}{h} \cdot \rho_f = \frac{f_c}{f_y} \cdot \frac{h_0}{h} \cdot \frac{\varepsilon_{cu} - \varepsilon_{co}/3}{\varepsilon_{cu} + \varepsilon_{etu}} - r_h \frac{f_{etc}}{f_y} \quad (18)$$

272 When maximum compressive concrete strain reaches the ultimate concrete compressive strain

273 and ECC/longitudinal reinforcement reach their ultimate tensile strain simultaneously, the following

274 equation can be obtained according to the plane section assumption.

$$\frac{\varepsilon_{cu} + \varepsilon_{hu,b}}{h_0} = \frac{\varepsilon_{cu} + \varepsilon_{etu}}{h} \quad (19)$$

275 Rearranging for  $\varepsilon_{hu,b}$ :

$$\varepsilon_{hu,b} = \frac{\varepsilon_{etu} h_0 - \varepsilon_{cu} h_s}{h} \quad (20)$$

276 When  $\varepsilon_{hu} \leq \varepsilon_{hu,b}$ , longitudinal reinforcement reaches the ultimate tensile strain first, failure mode

277 ① occurs for  $\zeta > \zeta_{cb1}$ , failure mode ② occurs for  $\zeta_{cb1} \leq \zeta \leq \zeta_{cb2}$  and failure mode ③ occurs for  $\zeta <$   
278  $\zeta_{cb2}$ . On the other hand, when  $\varepsilon_{hu} > \varepsilon_{hu,b}$ , ECC reinforcement reaches the ultimate tensile strain first,  
279 failure mode ① occurs for  $\zeta > \zeta_{cb1}$ , failure mode ② occurs for  $\zeta_{cb1} \leq \zeta \leq \zeta_{cb3}$  and failure mode ④  
280 occurs for  $\zeta < \zeta_{cb3}$ . For this investigation, as  $\varepsilon_{hu} = 0.0250 > \varepsilon_{hu,b} = 0.0215$ , ECC reaches their ultimate  
281 tensile strain before longitudinal reinforcement.

282 So appropriate reinforcements should meet the following requirements simultaneously:

$$\rho_s + \frac{E_f}{f_y} \cdot \frac{h_0 \varepsilon_{etu} - h_s \varepsilon_{cu}}{h} \cdot \rho_f \geq \frac{f_c}{f_y} \cdot \frac{h_0}{h} \cdot \frac{\varepsilon_{cu} - \varepsilon_{co}/3}{\varepsilon_{cu} + \varepsilon_{etu}} - r_h \frac{f_{etc}}{f_y} \quad (21)$$

$$\rho_{h,E} = \rho_s + \frac{E_f}{E_s} \rho_f \leq \frac{f_c}{f_y} \cdot \frac{\varepsilon_{cu} - \varepsilon_{co}/3}{\varepsilon_{cu} + \varepsilon_{sy}} - r_h \frac{f_{etc}}{f_y} \quad (22)$$

### 283 Cross-section analysis of composite beams

284 The following assumptions have been considered:

285 ·The steel bars and concrete/ECC have perfect bond and no delamination between ECC and  
286 concrete is considered as observed in the experimental investigations presented above or  
287 others in the literature (Yuan et al. 2013).

288 ·Each plane cross section perpendicular to the axis of the beam remains plane after loading.

289 ·The whole loading process can be divided into three stages as observed in the experimental  
290 investigations:

- 291 1. Elastic stage (uncracked section): from being loaded to cracking (ECC or concrete).
- 292 2. Working stress stage: from cracking to yielding of steel bars.
- 293 3. Failure stage: from yielding of steel bars to the failure of composite beams (i.e. any material  
294 reaches its ultimate strain: (a). Compressive strain in concrete reaches  $\varepsilon_{cu}$ . (b). Tensile strain in ECC  
295 reaches  $\varepsilon_{etu}$ . (c). Tensile strain in steel bars reaches  $\varepsilon_{su}$ . (d). Tensile strain in FRP bars reaches  $\varepsilon_{fu}$ ).

296 **Cracking moment**

297 The cross-section stress-strain distribution of elastic stage is shown in figure 16, where  $x$  is the  
 298 vertical distance of any point to the tensile edge of cross-section.

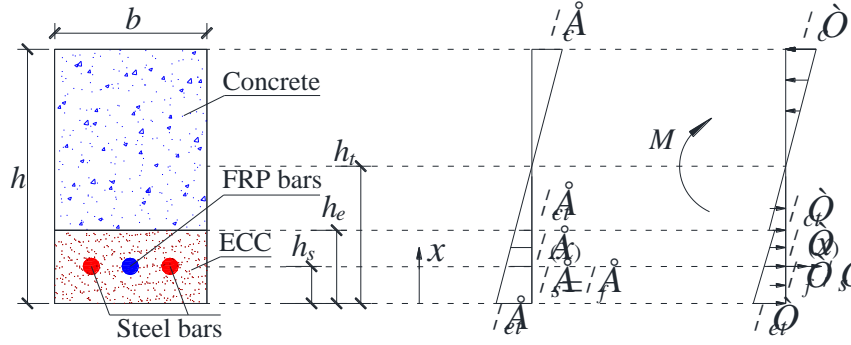


Fig.16 Cross-section stress-strain distribution of elastic stage

299 The cross-section strain distribution can be expressed as:

$$\varepsilon(x) = \begin{cases} (1-x/h_t)\varepsilon_{et} & , 0 \leq x \leq h_t \\ (x/h_t - 1)\varepsilon_{et} & , h_t < x \leq h \end{cases} \quad (23)$$

300 According to the force equilibrium of cross-section,  $\sum N = 0$ , the following equation can be  
 301 obtained,

$$\int_0^{h_e} \sigma_{ct}(x) b dx + \int_{h_e}^{h_t} \sigma_{ct}(x) b dx + E_s \varepsilon_s A_s + E_f \varepsilon_f A_f = \int_{h_t}^h \sigma_c(x) b dx \quad (24)$$

302 If ECC cracks before concrete, the maximum ECC tensile strain  $\varepsilon_{et} = \varepsilon_{etc}$ . Similarly,  $h_t$ ,  $\varepsilon_{ct}$ ,  $\varepsilon_s$  and  
 303  $\varepsilon_f$  can be expressed by variable  $\varepsilon_c$ ,  $h_t = \varepsilon_{etc} h / (\varepsilon_c + \varepsilon_{etc})$ ,  $\varepsilon_s = \varepsilon_f = \varepsilon_{etc} - (\varepsilon_c + \varepsilon_{etc}) h_s / h$ ,  $\varepsilon_{ct} = \varepsilon_{etc} - (\varepsilon_c +$   
 304  $\varepsilon_{etc}) h_e / h$ .

305 On the other hand, if concrete cracks before ECC, the maximum tensile strain in concrete  $\varepsilon_{ct} =$   
 306  $\varepsilon_{ctu}$ . Assuming  $\varepsilon_c$  as a basic variable,  $h_t$ ,  $\varepsilon_{et}$ ,  $\varepsilon_s$  and  $\varepsilon_f$  can be expressed by variable  $\varepsilon_c$ ,  $h_t = (h \varepsilon_{ctu} + h_e \varepsilon_c)$   
 307  $/ (\varepsilon_c + \varepsilon_{ctu})$ ,  $\varepsilon_s = \varepsilon_f = ((h - h_s) \varepsilon_{ctu} + (h_e - h_s) \varepsilon_c) / (h - h_e)$ ,  $\varepsilon_{et} = h (\varepsilon_{ctu} + \varepsilon_c) / (h - h_e) - \varepsilon_c$ .

308 Substituting  $\varepsilon_c$ ,  $h_t$ ,  $\varepsilon_{et}$ ,  $\varepsilon_{ct}$ ,  $\varepsilon_s$  and  $\varepsilon_f$  into formula (21), then concrete compressive strain  $\varepsilon_c$  can be  
 309 calculated. And then, according to the moment equilibrium of cross-section,  $\sum M = 0$ , cracking

310 moment formula can be expressed as below:

$$M_{cr} = \int_{h_c}^h \sigma_c(x) b x dx - \int_0^{h_e} \sigma_{et}(x) b x dx - \int_{h_e}^{h_i} \sigma_{ct}(x) b x dx - (E_s \varepsilon_s A_s + E_f \varepsilon_f A_f) h_s \quad (25)$$

311 Comparisons of cracking modes and cracking moments are shown in table 5.

312 Table 5 Comparison of experimental and predicted cracking moments

Beam notation	$M_{cr,e}$ (kN·m)	$M_{cr,c}$ (kN·m)	$M_{cr,c} / M_{cr,e}$	CM-E	CM-D	CM-A
HB1	3.26	3.08	0.95	—	—	—
HB2	3.74	3.70	0.94	C	C	C
HB3	3.75	3.67	0.94	E	E	E
HB5	3.26	3.20	0.98	—	—	—
HC1	3.26	3.15	0.97	—	—	—
HC2	4.00	3.75	0.94	C	C	C
HC3	3.74	3.72	1.00	E	E	E
HC5	3.56	3.35	0.94	—	—	—
HD1	3.00	2.89	0.96	—	—	—
HD2	3.26	3.20	0.98	E	C	C
HD3	3.25	3.13	0.96	E	E	E
HD5	3.00	2.79	0.93	—	—	—
HE1	3.02	2.96	0.98	—	—	—
HE2	3.39	3.33	0.99	C	C	C
HE3	3.71	3.28	0.88	E	E	E
HE5	3.23	2.93	0.91	—	—	—
HF1	3.26	3.02	0.93	—	—	—
HF2	3.75	3.48	0.93	C	C	C
HF3	3.77	3.43	0.91	E	E	E
HF5	3.33	3.06	0.92	—	—	—
HG1	3.46	3.15	0.91	—	—	—
HG2	3.82	3.75	0.98	C	C	C
HG3	3.80	3.72	0.98	E	E	E
HG5	3.55	3.35	0.94	—	—	—
HH1	3.49	3.15	0.90	—	—	—
HH2	3.75	3.75	1.00	C	C	C
HH3	3.99	3.72	0.93	E	E	E
HH5	3.59	3.35	0.93	—	—	—
HK1	3.02	2.77	0.92	—	—	—
HK2	3.97	3.75	0.93	E	C	C
HK3	3.66	3.72	0.93	E	E	E
HK5	3.73	3.51	0.94	—	—	—
Average values			0.95			
Variation coefficient			0.03			

313 Note:  $M_{cr,e}$  is experimental cracking moment,  $M_{cr,c}$  is calculated cracking moment, CM-E is experimental cracking  
 314 mode, CM-D is cracking mode based on the discriminate formula, CM-A is cracking mode based on cross-section  
 315 analysis, E means ECC cracking first and C means concrete cracking first, specimen HD2 has initial crack on layer  
 316 of ECC.

317 As can be seen from table 5, average values and variation coefficient of  $M_{cr,c} / M_{cr,e}$  are 0.95 and  
 318 0.03, respectively, indicating good agreement between the predicted and experimental results. The  
 319 predictions of the first crack location, i.e. in ECC or concrete first, from discriminate formula and  
 320 cross-section analysis are in good agreement with that observed in experiments, except for specimen  
 321 HD2 that initially cracked in ECC.

322 **Yield moment**

323 The cross-section stress-strain distribution for this case is shown in figure 17.

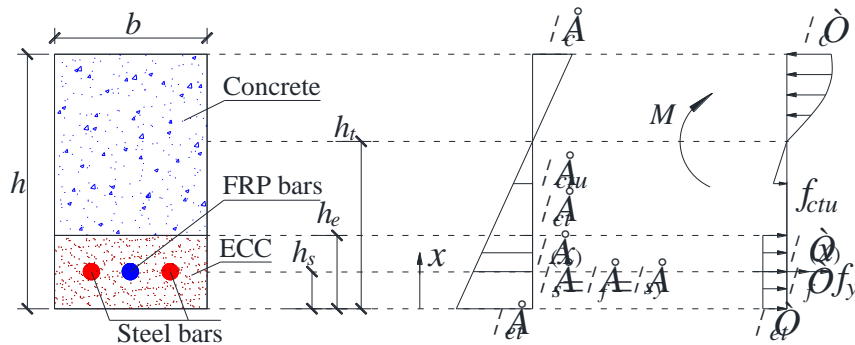


Fig.17 Cross-section stress-strain distribution of composites beams when steel yielded

324 In this situation, the tensile strain in steel bars  $\varepsilon_s = \varepsilon_f = \varepsilon_{sy}$ . Assuming  $\varepsilon_c$  as a basic variable,  $h_t$ ,  $\varepsilon_{ct}$   
 325 and  $\varepsilon_{ct}$  can be expressed in terms of  $\varepsilon_c$ ,  $h_t = \varepsilon_{sy} (h - h_s) / (\varepsilon_c + \varepsilon_{sy}) + h_s$ ,  $\varepsilon_{ct} = \varepsilon_{sy} + (\varepsilon_c + \varepsilon_{sy}) h_s / (h - h_s)$ ,  
 326  $\varepsilon_{ct} = \varepsilon_{sy} - (\varepsilon_c + \varepsilon_{sy}) (h_e - h_s) / (h - h_s)$ .

327 According to the force equilibrium of cross-section,  $\sum N = 0$ , the following equation can be  
 328 obtained,

$$\int_0^{h_e} \sigma_{ct}(x) b dx + \int_{h_e}^{h_t} \sigma_{ct}(x) b dx + f_y A_s + E_f \varepsilon_f A_f = \int_{h_t}^h \sigma_c(x) b dx \quad (26)$$

329 Substituting  $\varepsilon_c$ ,  $h_t$ ,  $\varepsilon_{ct}$ ,  $\varepsilon_{sy}$  and  $\varepsilon_{ct}$  into formula (23), then concrete compressive strain  $\varepsilon_c$  can be  
330 calculated. According to the moment equilibrium of cross-section,  $\sum M = 0$ , the yield moment can,  
331 then, be expressed as below:

$$M_y = \int_{h_t}^h \sigma_c(x) b x dx - \int_0^{h_e} \sigma_{ct}(x) b x dx - \int_{h_e}^{h_t} \sigma_{ct}(x) b x dx - (f_y A_s + E_f \varepsilon_{sy} A_f) h_s \quad (27)$$

332 Comparisons of experimental and predicted yield moments are shown in table 6.

333 Table 6 Comparison of experimental and predicted yield moments

Beam notation	$M_{y,e}$ (kN·m)	$M_{y,c}$ (kN·m)	$M_{y,c} / M_{y,e}$	Beam notation	$M_{y,e}$ (kN·m)	$M_{y,c}$ (kN·m)	$M_{y,c} / M_{y,e}$
HB1	14.7	13.3	0.90	HF1	8.71	10.8	1.24
HB2	16.2	15.5	0.96	HF2	11.2	13.0	1.16
HB3	17.9	16.8	0.94	HF3	12.4	14.4	1.16
HB5	17.4	15.7	0.90	HF5	12.4	15.0	1.21
HC1	14.0	12.9	0.92	HG1	17.3	14.8	0.86
HC2	17.4	15.2	0.87	HG2	17.5	16.9	0.97
HC3	19.6	16.5	0.84	HG3	18.8	18.9	1.01
HC5	16.9	16.2	0.96	HG5	18.4	18.7	1.02
HD1	7.02	6.83	0.97	HH1	19.5	18.9	0.97
HD2	9.45	9.14	0.97	HH2	23.2	21.1	0.91
HD3	10.7	10.6	0.99	HH3	23.9	22.4	0.94
HD5	10.7	11.3	1.06	HH5	23.7	22.5	0.95
HE1	9.28	8.94	0.96	HK1	—	—	—
HE2	14.0	11.2	0.80	HK2	—	—	—
HE3	13.4	12.6	0.94	HK3	—	—	—
HE5	13.7	13.3	0.97	HK5	—	—	—

334 Note:  $M_{y,e}$  is the experimental yield moment whereas  $M_{y,c}$  is the calculated yield moment.

335 As can be seen from table 5, average values and variation coefficient of  $M_{y,c} / M_{y,e}$  are 0.98 and  
336 0.10, respectively, indicating good agreement between the predicted and experimental yield  
337 moments.

### 338 *Ultimate moment*

339 The cross-section stress-strain distribution when concrete is crushed is shown in figure 18.

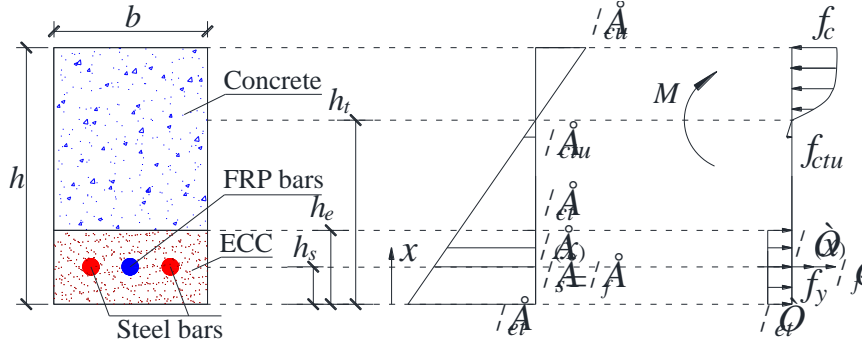


Fig.18 Cross-section stress-strain distribution – when concrete crushed after steel yielding

340 In this situation, the maximum compressive strain in concrete  $\varepsilon_c = \varepsilon_{cu}$ . Assuming  $\varepsilon_{et}$  as a basic  
 341 variable,  $h_t$ ,  $\varepsilon_{ct}$ ,  $\varepsilon_s$  and  $\varepsilon_f$  can be expressed in terms of  $\varepsilon_{et}$ ,  $h_t = \varepsilon_{et} h / (\varepsilon_{cu} + \varepsilon_{et})$ ,  $\varepsilon_s = \varepsilon_f = \varepsilon_{et} - (\varepsilon_{cu} + \varepsilon_{et}) h_s$   
 342  $/ h$ ,  $\varepsilon_{ct} = \varepsilon_{et} - (\varepsilon_{cu} + \varepsilon_{et}) h_e / h$ .

343 Substituting  $\varepsilon_c$ ,  $h_t$ ,  $\varepsilon_{et}$ ,  $\varepsilon_s$ ,  $\varepsilon_f$  and  $\varepsilon_{ct}$  into formula (23), then, the maximum ECC tensile strain  $\varepsilon_{et}$   
 344 can be calculated. According to the moment equilibrium of cross-section,  $\sum M = 0$ , ultimate moment  
 345 can, then, be expressed as below:

$$M_u = \int_{h_t}^h \sigma_c(x) b x dx - \int_0^{h_e} \sigma_{ct}(x) b x dx - \int_{h_e}^{h_t} \sigma_{ct}(x) b x dx - (f_y A_s + E_f \varepsilon_f A_f) h_s \quad (28)$$

346 If the composite beam is over-reinforced, steel bar does not yield while the concrete  
 347 compressive strain reaches the ultimate compressive strain and the beam incurs brittle failure. In this  
 348 case,  $\varepsilon_s = \varepsilon_f \leq \varepsilon_{sy}$ . Assuming  $\varepsilon_{et}$  as a basic variable,  $h_t$ ,  $\varepsilon_{ct}$ ,  $\varepsilon_s$  and  $\varepsilon_f$  can be expressed by variable  $\varepsilon_{et}$ ,  $h_t$   
 349  $= \varepsilon_{et} h / (\varepsilon_{cu} + \varepsilon_{et})$ ,  $\varepsilon_s = \varepsilon_f = \varepsilon_{et} - (\varepsilon_{cu} + \varepsilon_{et}) h_s / h$ ,  $\varepsilon_{ct} = \varepsilon_{et} - (\varepsilon_{cu} + \varepsilon_{et}) h_e / h$ . Substituting  $\varepsilon_c$ ,  $h_t$ ,  $\varepsilon_{et}$ ,  $\varepsilon_s$ ,  $\varepsilon_f$   
 350 and  $\varepsilon_{ct}$  into formula (21), then the maximum ECC tensile strain  $\varepsilon_{et}$  can be calculated. According to  
 351 the equilibrium of cross-section moment  $\sum M = 0$ , the ultimate moment can, then, be expressed as  
 352 below:

$$M_u = \int_{h_t}^h \sigma_c(x) b x dx - \int_0^{h_e} \sigma_{ct}(x) b x dx - \int_{h_e}^{h_t} \sigma_{ct}(x) b x dx - (E_s \varepsilon_s A_s + E_f \varepsilon_f A_f) h_s \quad (29)$$

353 If steel bars reach their ultimate tensile strain first, the tensile strain in bars  $\varepsilon_s = \varepsilon_f = \varepsilon_{su}$ ,  $h_t = \varepsilon_{su} (h$   
 354  $- h_s) / (\varepsilon_c + \varepsilon_{su}) + h_s$ ,  $\varepsilon_{ct} = \varepsilon_{su} + (\varepsilon_c + \varepsilon_{su}) h_s / (h - h_s)$ ,  $\varepsilon_{ct} = \varepsilon_{su} - (\varepsilon_c + \varepsilon_{su}) (h_e - h_s) / (h - h_s)$ . Substituting

355  $\varepsilon_c, h_t, \varepsilon_{et}, \varepsilon_s, \varepsilon_f$  and  $\varepsilon_{ct}$  into formula (23), then concrete compressive strain  $\varepsilon_c$  can be calculated.

356 According to the equilibrium of cross-section moment  $\sum M = 0$ , the ultimate moment can, then, be

357 expressed as below:

$$M_u = \int_{h_t}^h \sigma_c(x) b x dx - \int_0^{h_e} \sigma_{et}(x) b x dx - \int_{h_e}^{h_t} \sigma_{ct}(x) b x dx - (f_y A_s + E_f \varepsilon_{su} A_f) h_s \quad (30)$$

358 If FRP bars rupture first, the tensile strain in bars  $\varepsilon_s = \varepsilon_f = \varepsilon_{fu}, h_t = \varepsilon_{fu} (h - h_s) / (\varepsilon_c + \varepsilon_{fu}) + h_s, \varepsilon_{ct} =$

359  $\varepsilon_{fu} + (\varepsilon_c + \varepsilon_{fu}) h_s / (h - h_s), \varepsilon_{ct} = \varepsilon_{fu} - (\varepsilon_c + \varepsilon_{fu}) (h_e - h_s) / (h - h_s)$ . Substituting  $\varepsilon_c, h_t, \varepsilon_{et}, \varepsilon_s, \varepsilon_f$  and  $\varepsilon_{ct}$  into

360 formula (23), then concrete compressive strain  $\varepsilon_c$  can be calculated. According to the equilibrium of

361 cross-section moment  $\sum M = 0$ , the ultimate moment can, then, be expressed as below:

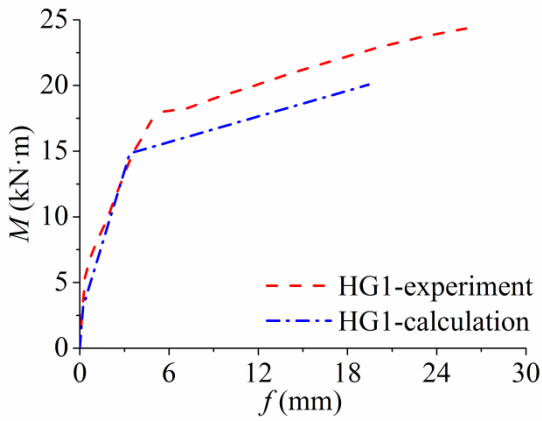
$$M_u = \int_{h_t}^h \sigma_c(x) b x dx - \int_0^{h_e} \sigma_{et}(x) b x dx - \int_{h_e}^{h_t} \sigma_{ct}(x) b x dx - (f_y A_s + f_u A_f) h_s \quad (31)$$

### 362 **Loading-deflection curves**

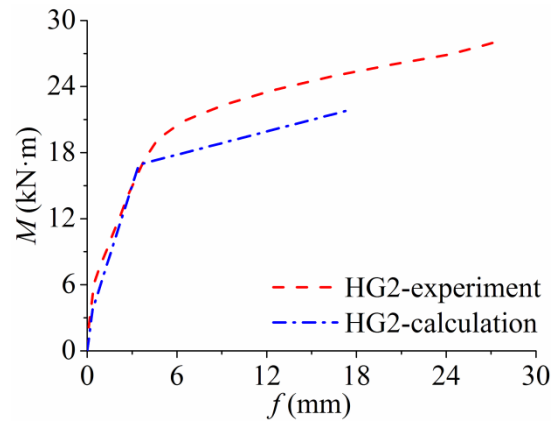
363 After the whole process of cross-section analysis of composite beams is completed, the

364 load-deflection curves of specimens can be obtained (Xu et al. 2009). The comparisons of

365 experimental and calculated load-deflection curves of group HG are shown in figure 19.



(a) HG1



(b) HG2

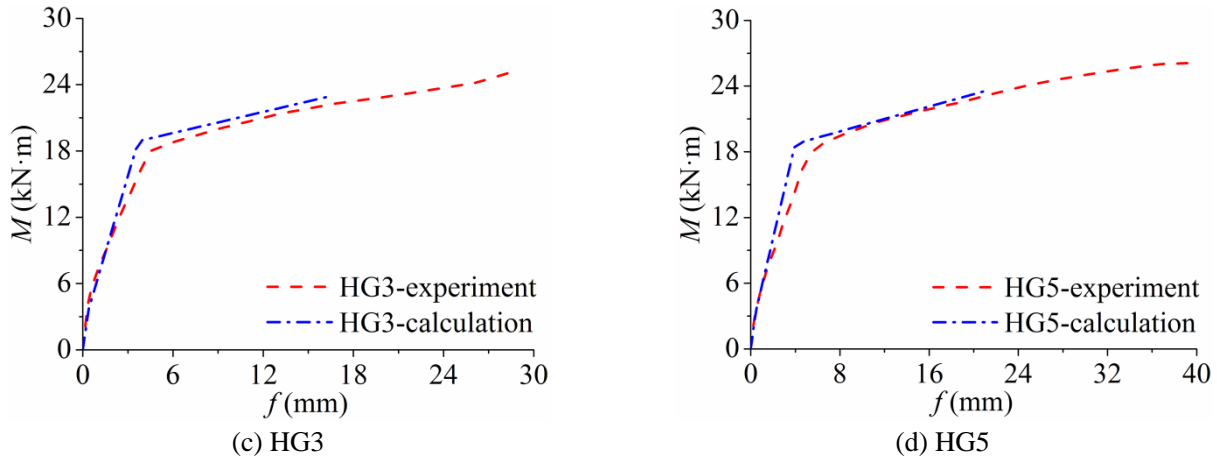


Fig.19 Comparisons of experimental and calculated moment-deflection curves

366 As can be seen from the figure 19, experimental and calculated curves fit well.

### 367 *Parametric study*

368 In this section of the paper, the effect of various parameters including the strength, height  
 369 replacement ratio and ultimate tensile strain of ECC, strength, elastic modulus and amount of  
 370 reinforcement, compressive strength and ultimate compressive strain of concrete on the flexural  
 371 behavior (cracking moment  $M_{cr}$ , yield moment  $M_y$ , ultimate moment  $M_u$ , yield curvature  $\varphi_y$ , ultimate  
 372 curvature  $\varphi_u$ , ductility  $u_\varphi$  and energy dissipation  $E_\varphi$ ) of FRP reinforced ECC-concrete composite  
 373 beams is considered.

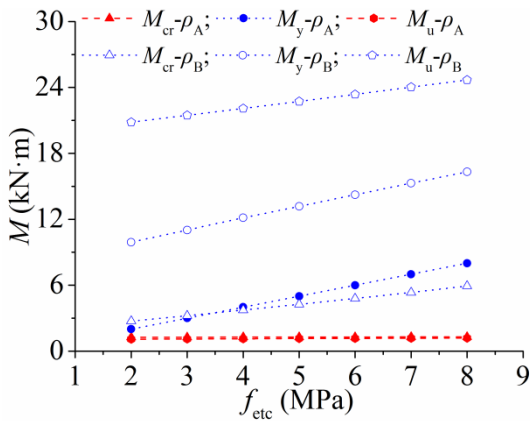
374 When one parameter is changed, other basic parameters are kept constant at the following  
 375 values: ECC height replacement ratio  $r_h$  is 0.29, reinforcement ratio are  $\rho_A$  ( $\rho_{s,A} + \rho_{f,A} = 0.6\% + 0.3\%$ )  
 376 and  $\rho_B$  ( $\rho_{s,B} + \rho_{f,B} = 0.3\% + 0.6\%$ ), respectively, yield strength of steel reinforcement  $f_{yk}$  is 400 MPa,  
 377 compressive strength of concrete  $f_c$  is 28.6 MPa and its ultimate compressive strain  $\varepsilon_{cu}$  is 0.0033,  
 378 ECC tensile strength at first cracking  $f_{etc}$  is 5.0 MPa and its corresponding strain  $\varepsilon_{etc}$  is 0.0003, ECC  
 379 ultimate tensile strength  $f_{etu}$  is 1.2 times of  $f_{etc}$  and its corresponding strain  $\varepsilon_{etu}$  is 0.03.

380 The composite beam cross-section is assumed to be failed when maximum concrete  
 381 compressive strain,  $\varepsilon_c$ , tensile strains in reinforcement,  $\varepsilon_s$ , or tensile strains in ECC,  $\varepsilon_{et}$ , reaches their

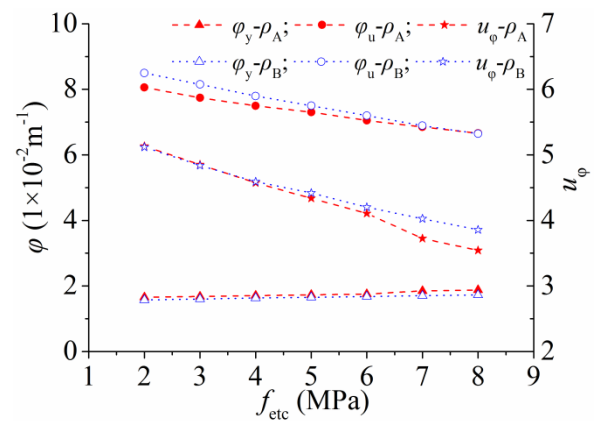
382 ultimate strain, respectively. The failure modes can be predicted by the proposed model, namely  
 383 failure mode ① (over-reinforced failure - concrete compressive strain reaches  $\varepsilon_{cu}$  before yielding of  
 384 steel reinforcement), failure mode ② (compressive failure - concrete compressive strain reaches  $\varepsilon_{cu}$   
 385 after yielding of steel reinforcement), failure mode ③ (tensile failure 1 - tensile strain in  
 386 reinforcement reaches  $\varepsilon_{hu}$  first) and failure mode ④ (tensile failure 2 - tensile strain in ECC reaches  
 387  $\varepsilon_{etu}$  first). All specimens occur compressive failure (failure mode ②) according to formulas (21) ~  
 388 (22).

### 389 I Strength, height replacement ratio and ultimate tensile strain of ECC

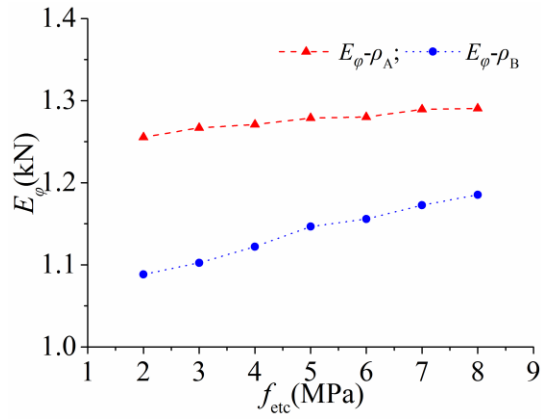
390 The effect of ECC strength, ECC height replacement ratio and ECC ultimate tensile strain on  
 391 the flexural behavior are shown in figures 20 ~ 22. Seven ECC tensile strengths  $f_{etc}$  (2.0 MPa, 3.0  
 392 MPa, 4.0 MPa, 5.0 MPa, 6.0 MPa, 7.0 MPa and 8.0 MPa), five ECC height replacement ratios  $r_h$  (0,  
 393 0.14, 0.29, 0.43 and 0.57) and five ECC ultimate tensile strains  $\varepsilon_{etu}$  (0.02, 0.03, 0.04, 0.05 and 0.06)  
 394 are studied.



(a) Cracking, yield and ultimate moment

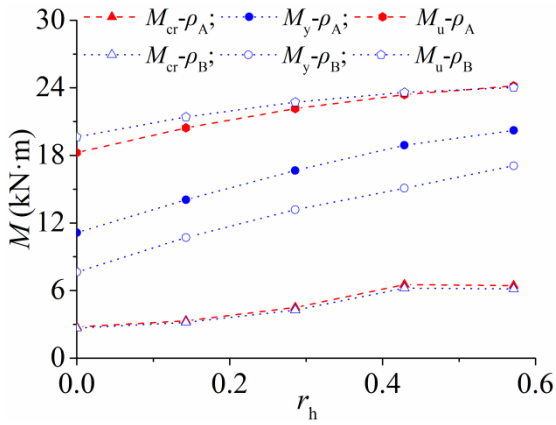


(b) Yield curvature, ultimate curvature and ductility

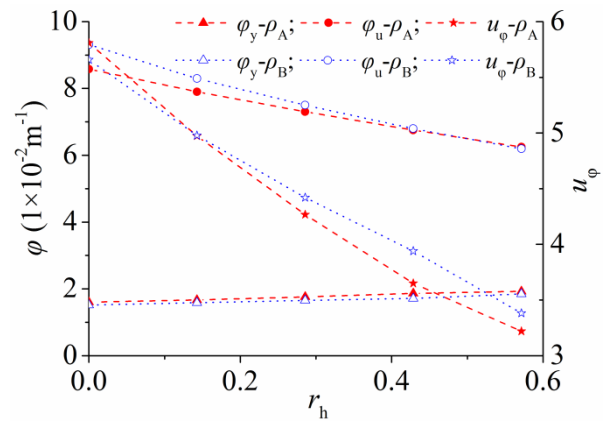


(c) Energy dissipation

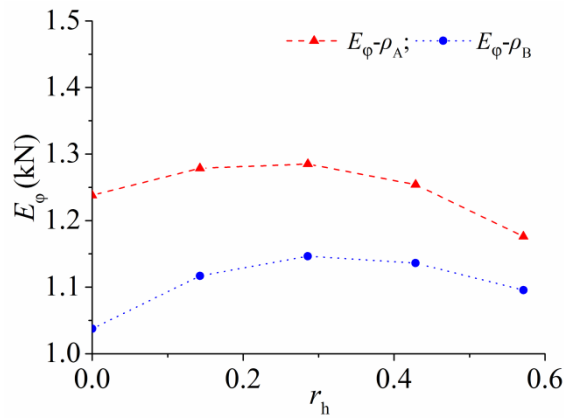
Fig.20 Effect of ECC strength



(a) Cracking, yield and ultimate moment

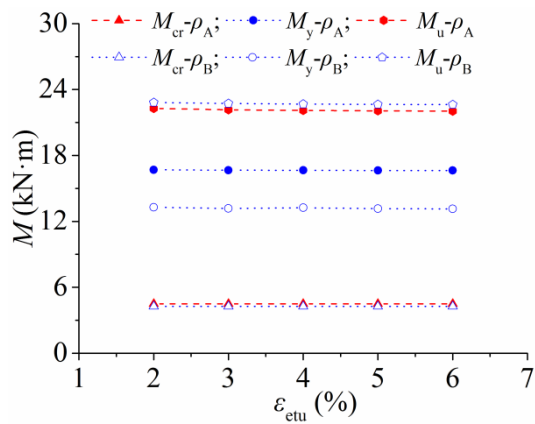


(b) Yield curvature, ultimate curvature and ductility

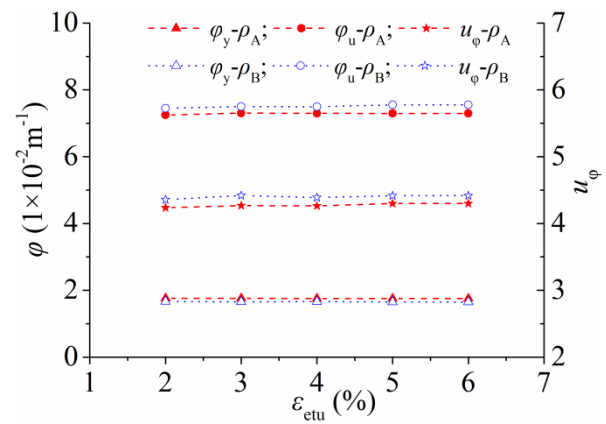


(c) Energy dissipation

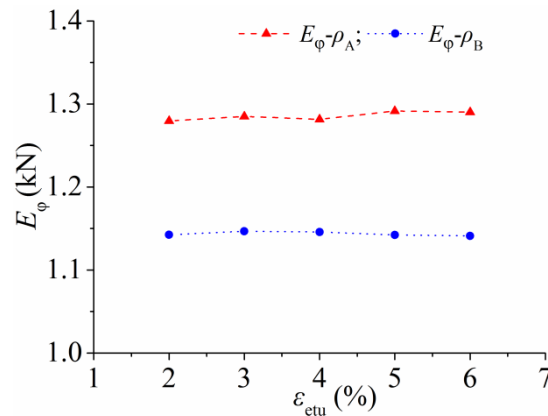
Fig.21 Effect of ECC height replacement ratio



(a) Cracking, yield and ultimate moment



(b) Yield curvature, ultimate curvature and ductility



(c) Energy dissipation

Fig.22 Effect of ECC ultimate tensile strain

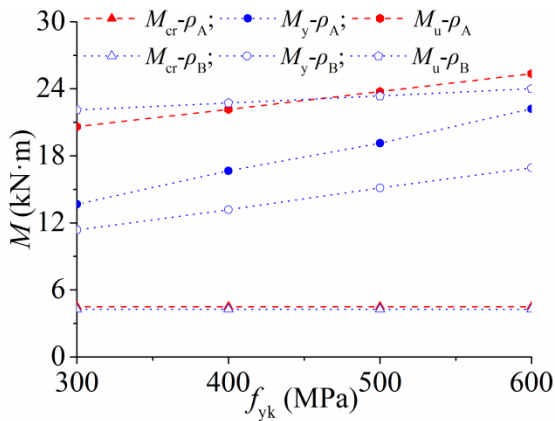
395 As can be seen from figures 20 and 21, the cracking, yield and ultimate moments increase with  
 396 increasing the strength or the height replacement ratio of ECC. The yield curvature gradually  
 397 increases while the ultimate curvature gradually decreases with increasing the strength or the height  
 398 replacement ratio of ECC. So, the curvature ductility decreases with increasing the strength or the  
 399 height replacement ratio of ECC. With increasing the strength of ECC, the energy dissipation  
 400 gradually increases. With increasing the height replacement ratio of ECC, the energy dissipation,  
 401 initially, increases and, then, decreases.

402 For all specimens compressive failure occurs (failure mode ②) - crushing of concrete after  
 403 yielding of steel reinforcement and, therefore, ECC ultimate tensile strain has no significant

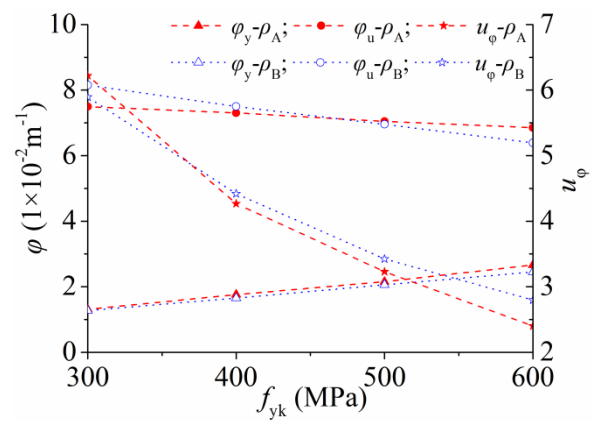
404 influence on the flexural behavior of composite beams as indicated in figure 22.

## 405 II Strength, elastic modulus and amount of reinforcement

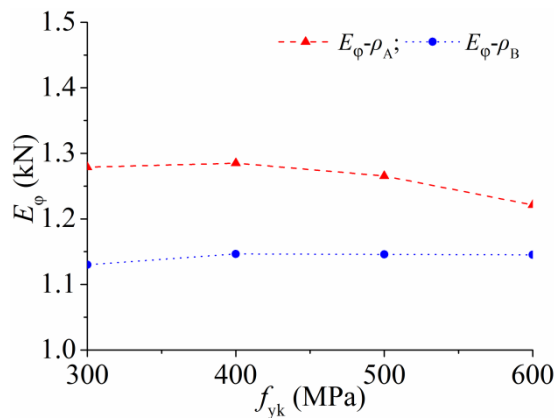
406 The effect of yield strength of steel reinforcement, ultimate tensile strength and elastic modulus  
 407 of FRP reinforcement, amount of reinforcement on the flexural behavior is shown in figures 23 ~ 26.  
 408 Four yield strengths of steel reinforcement  $f_{yk}$  (300 MPa, 400 MPa, 500 MPa and 600 MPa), four  
 409 elastic moduli of FRP reinforcement  $E_f$  (50 GPa, 75 GPa, 100 GPa and 125 GPa), five ultimate  
 410 tensile strengths of FRP reinforcement  $f_{fu}$  (600 MPa, 900 MPa, 1200 MPa, 1500 MPa and 1800 MPa)  
 411 and three groups of reinforcement (group 1:  $\rho_h = 0.6\%$ ,  $\rho_{h,E} = 0.15\%$ ,  $0.3\%$  and  $0.60\%$ ,  
 412 respectively; group 2:  $\rho_h = 0.9\%$ ,  $\rho_{h,E} = 0.22\%$ ,  $0.45\%$ ,  $0.67\%$  and  $0.90\%$ , respectively; group 3:  $\rho_h$   
 413  $= 1.2\%$ ,  $\rho_{h,E} = 0.52\%$ ,  $0.75\%$  and  $0.97\%$ , respectively) are studied.



(a) Cracking, yield and ultimate moment

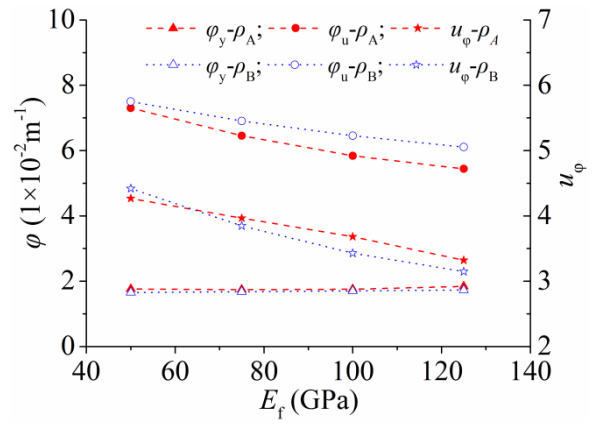
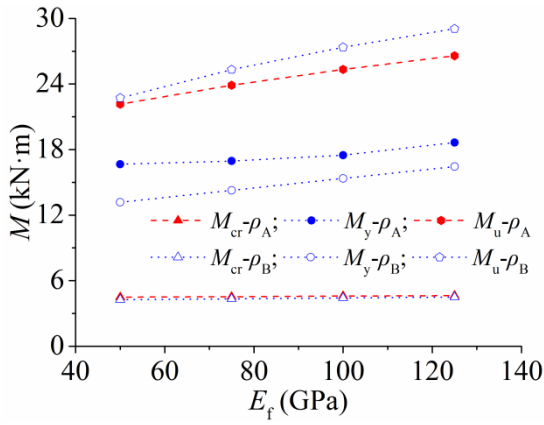


(b) Yield curvature, ultimate curvature and ductility



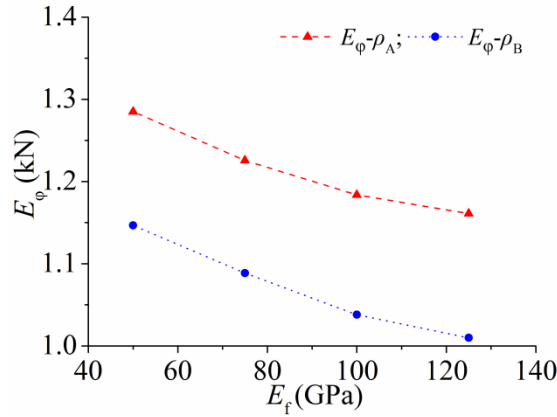
(c) Energy dissipation

Fig.23 Effect of steel yield strength



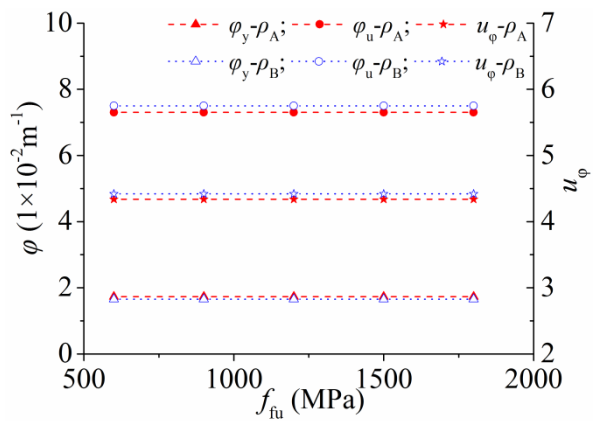
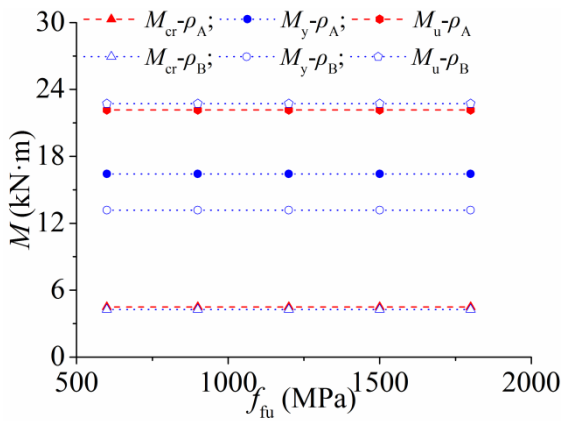
(a) Cracking, yield and ultimate moment

(b) Yield curvature, ultimate curvature and ductility



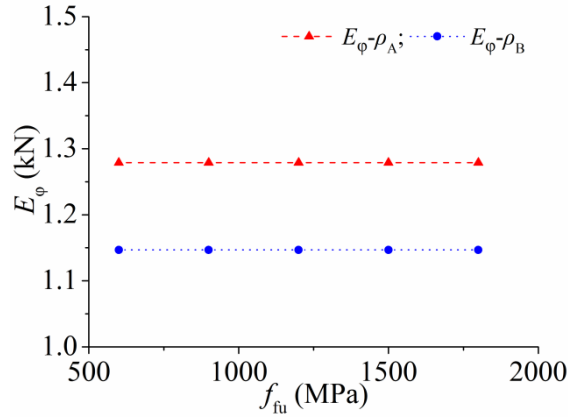
(c) Energy dissipation

Fig.24 Effect of FRP elastic modulus



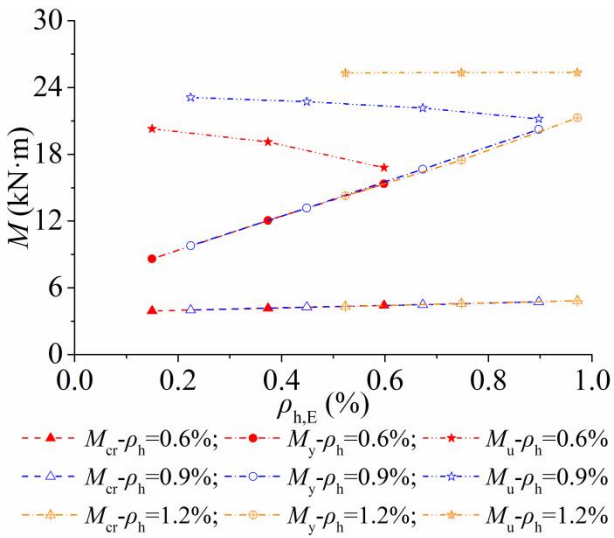
(a) Cracking, yield and ultimate moment

(b) Yield curvature, ultimate curvature and ductility

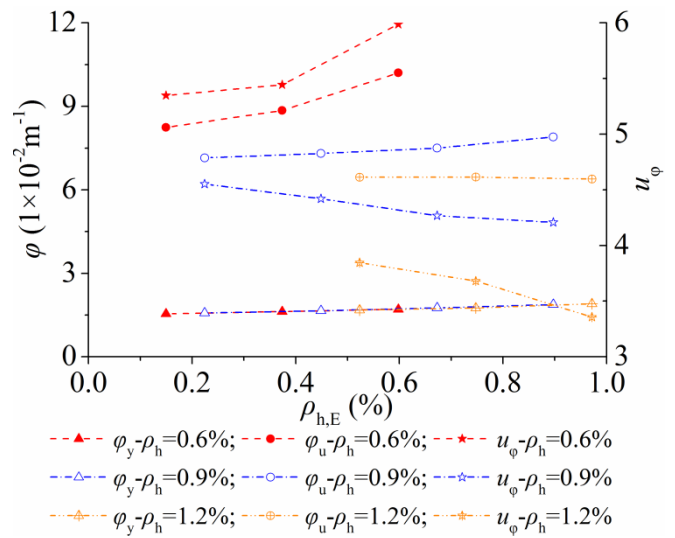


(c) Energy dissipation

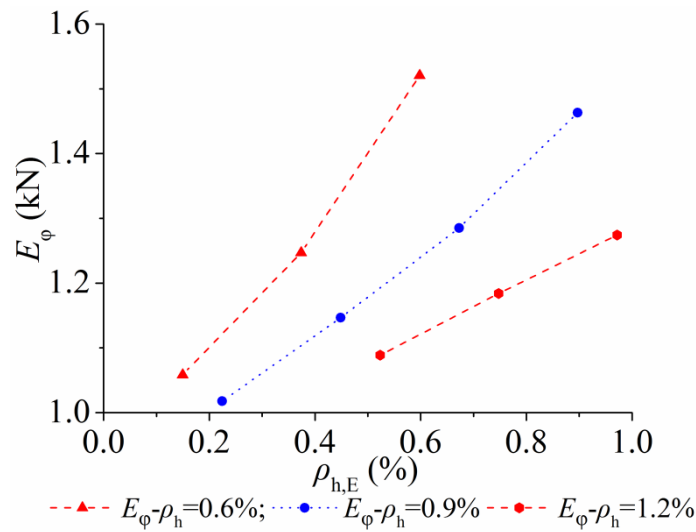
Fig.25 Effect of FRP ultimate tensile strength



(a) Cracking, yield and ultimate moment



(b) Yield curvature, ultimate curvature and ductility



(c) Energy dissipation

Fig.26 Effect of the nominal reinforcement ratio using elastic modulus conversion ratio

414 As can be seen from figures 23 ~ 26, the yield and ultimate moments increase with increasing  
415 the yield strength of steel reinforcement or the elastic modulus of FRP reinforcement. The cracking  
416 moments slightly increase with increasing the elastic modulus of FRP reinforcement while the yield  
417 strength of steel reinforcement has no effect on the cracking moment.

418 With increasing the yield strength of steel reinforcement or the elastic modulus of FRP  
419 reinforcement, the yield curvature gradually increases while the ultimate curvature gradually  
420 decreases, and the curvature ductility decreases accordingly. With increasing the yield strength of  
421 steel reinforcement, the energy dissipation, initially, increases and, then, decreases. With increasing  
422 the elastic modulus of FRP reinforcement, the energy dissipation gradually decreases.

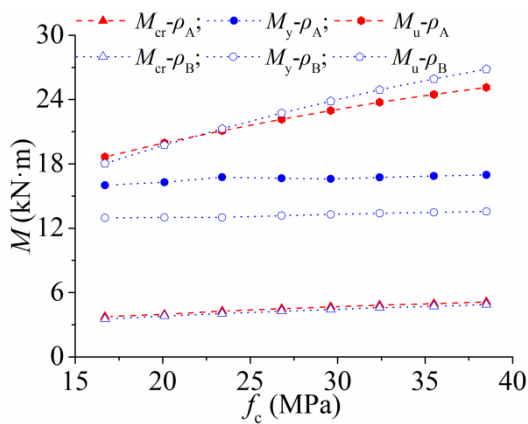
423 For all specimens compressive failure occurs (failure mode ②) - crushing of concrete after  
424 yielding of steel reinforcement and, therefore, the ultimate tensile strength of FRP reinforcement has  
425 no effect on the flexural behavior of composite beams as presented in figure 25.

426 With increasing the nominal reinforcement ratio using elastic modulus conversion ratio,  
427 cracking moment slightly increases, the yield moment significantly increases and the ultimate  
428 moment gradually decreases. The ultimate moment decreasing rate decreases with the increase of the  
429 practical reinforcement ratio. The yield curvature and ultimate curvature gradually increase, and the  
430 ultimate curvature increasing rate decreases with increasing the practical reinforcement ratio. The  
431 curvature ductility of specimens with lower practical reinforcement ratio (group 1) increases while  
432 curvature ductility of specimens with higher practical reinforcement ratio (group 2 and 3) decreases  
433 with increasing the nominal reinforcement ratio using elastic modulus conversion ratio. The energy  
434 dissipation gradually increases with increasing the nominal reinforcement ratio using elastic modulus

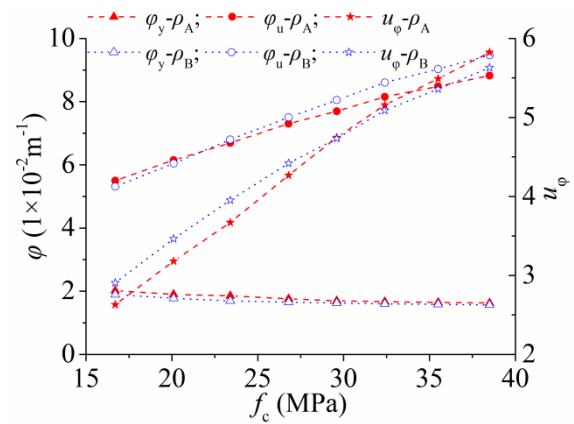
435 conversion ratio.

### 436 III Compressive strength and ultimate compressive strain of concrete

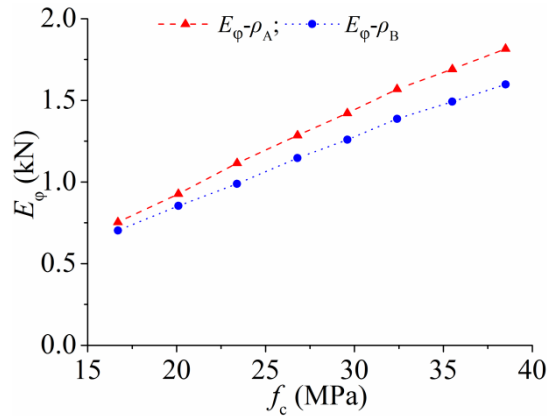
437 The effect of concrete compressive strength and ultimate compressive strain on the flexural  
 438 behavior is shown in figures 27 ~ 28. Eight concrete strengths  $f_c$  (16.7 MPa, 20.1 MPa, 23.4 MPa,  
 439 26.8 MPa, 29.6 MPa, 32.4 MPa, 35.5 MPa and 38.5 MPa) and four concrete ultimate compressive  
 440 strains  $f_{fu}$  (0.003, 0.0035, 0.004 and 0.005) are studied.



(a) Cracking, yield and ultimate moment

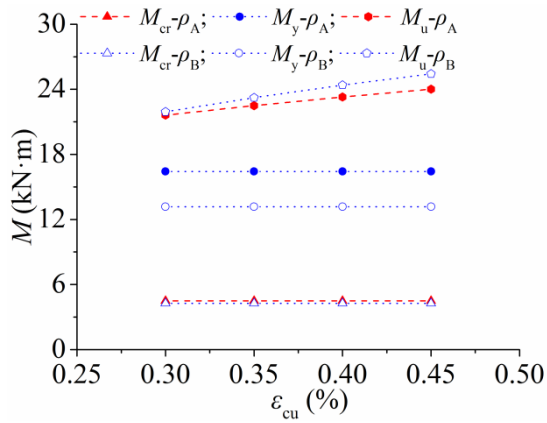


(b) Yield curvature, ultimate curvature and ductility

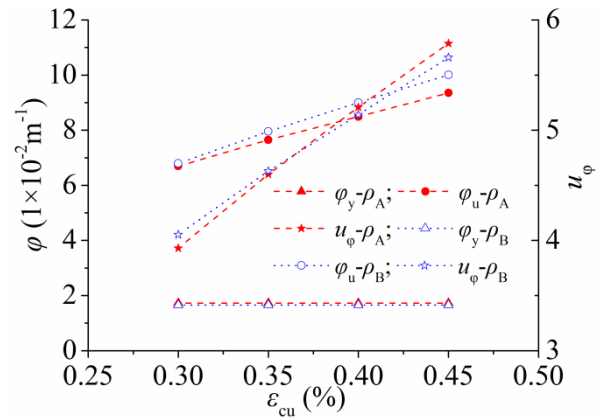


(c) Energy dissipation

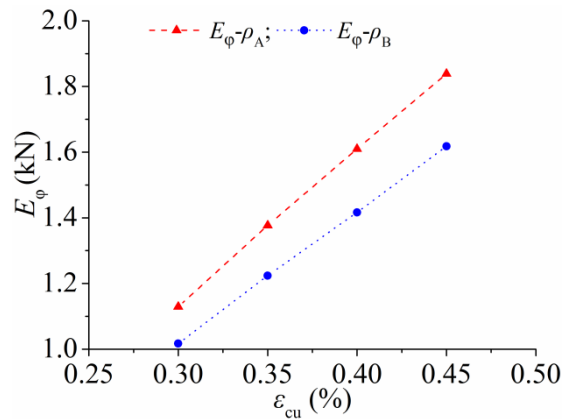
Fig.27 Effect of concrete compressive strength



(a) Cracking, yield and ultimate moment



(b) Yield curvature, ultimate curvature and ductility



(c) Energy dissipation

Fig.28 Effect of concrete ultimate compressive strain

441 As can be seen from figures 27 and 28, the cracking, yield and ultimate moments increase with  
 442 the increase of the strength of concrete. With increasing the concrete ultimate compressive strain, the  
 443 ultimate moments gradually increase while the cracking and yield moments keep constant.

444 The yield curvature slightly decreases with increasing the concrete compressive strength while  
 445 concrete ultimate compressive strain has no effect on the yield curvature. The ultimate curvature  
 446 significantly increases with increasing the concrete compressive strength. So, the curvature ductility  
 447 and the energy dissipation significantly increase with increasing the concrete compressive strength.

#### 448 Simplified calculation of ultimate moment

449 In this section, a simplified calculation of section ultimate moment is developed. It is mainly

450 based on a simplified rectangular stress block of concrete stresses in compression and ECC in  
 451 tension. Two cases are proposed as explained below.

452 **Hybrid reinforced ECC-concrete composite beams**

453 The simplified cross-section stress-strain distribution when the appropriate hybrid reinforced  
 454 composite beam incurs failure is shown in figure 29. The following formula can be obtained  
 455 according to the force equilibrium of cross-section, where  $x_c$  and  $x$  are the actual and height of  
 456 compressive concrete, respectively,  $x = \beta_c x_c$ ,  $\alpha_c$  and  $\beta_c$  are coefficients related to the properties of  
 457 concrete (Chinese National Standard 2010),  $\alpha_c = 1.0$  and  $\beta_c = 0.8$ .

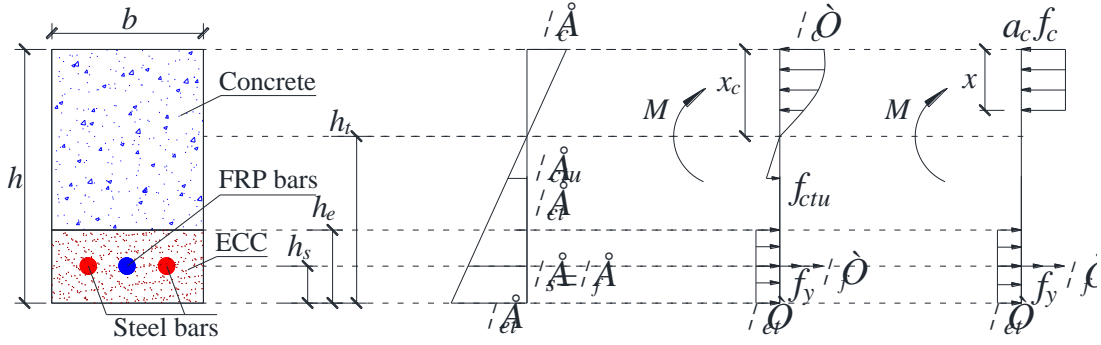


Fig.29 Simplified stress distribution of hybrid reinforced composite beam at failure

$$\alpha_c f_c b x = f_y A_s + E_f \varepsilon_{fu} A_f + f_{etc} b h_e \quad (32)$$

$$\varepsilon_{fu} = \varepsilon_{cu} (\beta_c / \xi - 1) \quad (33)$$

458 Combining equations (32) and (33), the flexural capacity of hybrid reinforced concrete beams  
 459 can be calculated by the following simplified formula:

$$\begin{aligned} M_u &= (f_y A_s + E_f \varepsilon_{fu} A_f) (1 - \xi_h / 2) h_0 + f_{etc} b h_e (h - h_e / 2 - \xi_h h_0 / 2) \\ &= \alpha_c f_c b h_0^2 \xi_h (1 - \xi_h / 2) - f_{etc} b h_e (h_e / 2 - h_s / 2) \end{aligned} \quad (34)$$

$$\xi_h = \frac{-B_h + \sqrt{B_h^2 - 4A_h C_h}}{2A_h} \quad (35)$$

460 where,  $A_h = \alpha_c f_c$ ,  $B_h = E_f \varepsilon_{cu} \rho_f - f_y \rho_s - f_{etc} r_h$ ,  $C_h = - E_f \rho_f \varepsilon_{cu} \beta_c$ .

461 As the tension of concrete is neglected when calculating the ultimate moment of concrete beams

462 (Chinese National Standard 2010), so the formula of ultimate moment of hybrid reinforced  
 463 composite beams can be also applied to hybrid reinforced concrete beams by just substituting  $f_{ect} = 0$ .

464 **Hybrid reinforced ECC beams**

465 When reinforced hybrid reinforced ECC beam incurs failure, the actual stress distribution and  
 466 simplified stress distribution of hybrid reinforced ECC beams are shown in figure 30. The following  
 467 formulas can be obtained according to force equilibrium of cross-section, where  $x_e$  and  $x$  are the  
 468 actual and calculate height of compressive ECC, respectively,  $x = \beta_e x_e$ ;  $\alpha_e$  and  $\beta_e$  are coefficients  
 469 related to the properties of ECC;  $F_{ec}$  is the resultant force of compressive ECC.

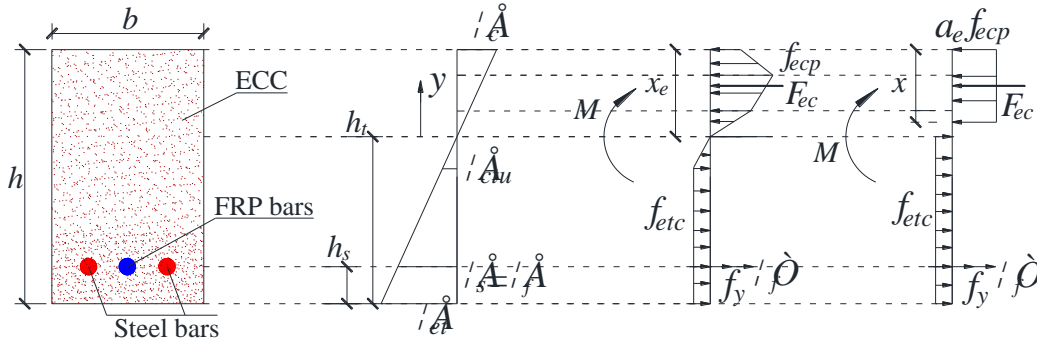


Fig.30 Simplified stress distribution of hybrid reinforced ECC beam at failure

$$\alpha_e f_{ecp} bx = f_y A_s + E_f \varepsilon_{hu} A_f + f_{etc} b h_t \quad (36)$$

$$\varepsilon_{hu} = \varepsilon_{ecu} (\beta_e / \xi - 1) \quad (37)$$

470 As the resultant stresses and the resultant moment of the compressive force to the neutral axils  
 471 of actual stress distribution are equal to those of simplified stress distribution, the following formulas  
 472 can be obtained,

$$\alpha_e f_{ecp} bx = \int_0^{x_e} \sigma_{ec}(y) b dy \quad (38)$$

$$\alpha_e f_{ecp} bx (x_e - x/2) = \int_0^{x_e} \sigma_{ec}(y) b y dy \quad (39)$$

473 Substituting the basic mechanical properties of ECC to equations (38) and (39),  $\alpha_e$  and  $\beta_e$  can be  
 474 obtained,  $\alpha_e = 1.0$  and  $\beta_e = 0.75$ .

475 And then, according to the moment equilibrium of cross-section,  $\sum M = 0$ , the flexural capacity  
 476 of hybrid reinforced ECC beams can be calculated by the following simplified formula:

$$\begin{aligned} M_u &= (f_y A_s + E_f \varepsilon_{fu} A_f)(1 - \xi_e / 2) h_0 + f_{etc} b h_e (h - h_e / 2 - \xi_e h_0 / 2) \\ &= \alpha_e f_{ecp} b h_0^2 \xi_e (1 - \xi_e / 2) - f_{etc} b h_e (h_e / 2 - h_s / 2) \end{aligned} \quad (40)$$

$$\xi_e = \frac{-B_e + \sqrt{B_e^2 - 4A_e C_e}}{2A_e} \quad (41)$$

477 where,  $A_e = \alpha_e f_{ecp}$ ,  $B_e = E_f \varepsilon_{ecu} \rho_f - f_{etc} r_h - f_y \rho_s$ ,  $C_e = -E_f \rho_f \varepsilon_{ecu} \beta_e$ .

478 Comparisons of experimental and calculated ultimate moments are shown in table 7.

479 Table 7 Comparison of ultimate experimental and predicted moments

Beam notation	$M_{u,e}$ (kN·m)	$M_{u,c1}$ (kN·m)	$M_{u,s1}$ (kN·m)	$M_{u,c2}$ (kN·m)	$M_{u,s2}$ (kN·m)	$M_{u,c1} / M_{u,e}$	$M_{u,s1} / M_{u,e}$	$M_{u,c2} / M_{u,e}$	$M_{u,s2} / M_{u,e}$	$M_{u,s1} / M_{u,c1}$	$M_{u,s2} / M_{u,c2}$
HB1	19.3	15.2	15.2	18.5	18.5	0.79	0.79	0.96	0.96	1.00	1.00
HB2	19.5	17.7	17.3	20.9	20.5	0.91	0.89	1.07	1.05	0.98	0.98
HB3	19.8	19.3	18.6	22.3	21.7	0.97	0.94	1.13	1.10	0.96	0.97
HB5	22.5	18.2	20.0	20.7	23.2	0.81	0.89	0.92	1.03	1.10	1.12
HC1	22.0	18.5	18.6	21.5	21.6	0.84	0.85	0.98	0.98	1.01	1.00
HC2	23.9	20.3	20.0	23.3	23.1	0.85	0.84	0.97	0.97	0.99	0.99
HC3	25.7	21.3	20.8	24.3	23.9	0.83	0.81	0.95	0.93	0.98	0.98
HC5	24.8	22.2	21.5	24.9	24.8	0.90	0.87	1.00	1.00	0.97	1.00
HD1	18.3	17.9	17.6	18.5	18.3	0.98	0.96	1.01	1.00	0.98	0.99
HD2	18.6	19.3	19.0	19.9	19.7	1.04	1.02	1.07	1.06	0.98	0.99
HD3	22.0	19.9	19.4	20.5	20.1	0.90	0.88	0.93	0.91	0.97	0.98
HD5	21.9	21.3	19.5	21.9	20.3	0.97	0.89	1.00	0.93	0.92	0.93
HE1	21.2	19.0	19.2	19.9	20.1	0.90	0.91	0.94	0.95	1.01	1.01
HE2	26.8	20.5	20.2	21.4	21.3	0.76	0.75	0.80	0.79	0.99	1.00
HE3	23.6	21.1	20.6	22.1	21.7	0.89	0.87	0.94	0.92	0.98	0.98
HE5	27.1	22.5	20.9	23.4	22.0	0.83	0.77	0.86	0.81	0.93	0.94
HF1	17.3	17.1	17.2	18.6	18.8	0.99	0.99	1.08	1.09	1.01	1.01
HF2	20.1	18.9	18.5	20.4	20.3	0.94	0.92	1.01	1.01	0.98	1.00
HF3	21.4	19.8	19.3	21.4	21.0	0.93	0.90	1.00	0.98	0.97	0.98
HF5	19.7	20.8	20.0	22.3	21.8	1.06	1.02	1.13	1.11	0.96	0.98
HG1	24.3	20.1	20.3	22.4	22.7	0.83	0.84	0.92	0.93	1.01	1.01
HG2	28.3	21.9	21.6	24.2	24.2	0.77	0.76	0.86	0.86	0.99	1.00
HG3	25.1	22.9	22.4	25.2	25.0	0.91	0.89	1.00	1.00	0.98	0.99
HG5	26.8	23.6	23.4	25.7	26.0	0.88	0.87	0.96	0.97	0.99	1.01
HH1	26.6	22.7	22.8	25.9	26.0	0.85	0.86	0.97	0.98	1.00	1.00
HH2	28.8	24.5	24.3	27.7	27.5	0.85	0.84	0.96	0.95	0.99	0.99

HH3	28.7	25.5	25.1	28.7	28.3	0.89	0.87	1.00	0.99	0.98	0.99
HH5	27.2	26.0	26.1	28.7	29.5	0.96	0.96	1.06	1.08	1.00	1.03
HK1	17.8	—	—	18.4	18.5	—	—	1.03	1.04	—	1.01
HK2	20.4	—	—	19.6	19.3	—	—	0.96	0.95	—	0.98
HK3	22.3	—	—	19.9	19.5	—	—	0.89	0.87	—	0.98
HK5	22.0	—	—	19.2	18.0	—	—	0.87	0.82	—	0.94
					<i>u</i>	0.89	0.88	0.98	0.97	0.99	0.99
					CV	0.08	0.08	0.08	0.08	0.03	0.03

480 Note:  $M_{u,e}$  is the experimental ultimate moment;  $M_{u,c1}$  and  $M_{u,c2}$  are the ultimate moment calculated by derived  
481 formula by using of yield strength and ultimate strength of steel bars, respectively;  $M_{u,s1}$  and  $M_{u,s2}$  are the ultimate  
482 moment calculated by simplified formula by using of yield strength and ultimate strength of steel bars, respectively.  
483  $u$  and CV are the average value and variation coefficient, respectively.

484 As can be observed from table 6, the average values of  $M_{u,c1} / M_{u,e}$  and  $M_{u,s1} / M_{u,e}$  are 0.89 and  
485 0.88, respectively, and their variation coefficients are 0.08 and 0.08, respectively. The ultimate  
486 moments calculated by derived and simplified formulas, when yield strength of steel bars used, are  
487 lower than the respective experimental ultimate moment for each beam tested. The average values of  
488  $M_{u,c2} / M_{u,e}$  and  $M_{u,s2} / M_{u,e}$  are 0.98 and 0.97, respectively, and their variation coefficients are 0.08  
489 and 0.08, respectively, indicating good agreement between the predicted and experimental results.  
490 The average values of  $M_{u,s1} / M_{u,c1}$  and  $M_{u,s2} / M_{u,c2}$  are 0.99 and 0.99, respectively, and their variation  
491 coefficients are 0.03 and 0.03, indicating good agreement between the calculated ultimate moments  
492 of derived formula and simplified formula and experimental results.

## 493 Conclusions

494 Experimental and analytical flexural behavior of hybrid composite beams reinforced with steel  
495 and FRP bars are studied. Based on the constitutive models of materials and plane-section  
496 assumption, simplified discriminate formulas of cracking mode are developed. Two boundary failure  
497 points and three failure modes of hybrid composite beams are proposed, and the discriminate

498 formulas of failure modes are also given. Furthermore, formulas for cracking, yield, ultimate  
499 moments are derived. Simplified flexural capacity formulas of hybrid reinforced composite beams  
500 and ECC beams are also proposed. Experimental results show that the proposed formulas are in good  
501 agreement with the experimental results, confirming the applicability of various formulas developed.  
502 The trend of flexural behavior of composite beams against the reinforcement, ECC and concrete  
503 properties has been developed based on a comprehensive parametric study. The following  
504 conclusions may be drawn:

- 505 • The cracking, yield and ultimate moments of composite beams and ECC beams are higher than  
506 these of conventional concrete beams, regardless of the reinforcement used. At the same load, the  
507 deflection of composite beams and ECC beams are less than that of conventional concrete beams,  
508 having the same amount of reinforcement.
- 509 • After yielding of steel reinforcement, the deflections of steel reinforced concrete beams,  
510 ECC-concrete composite beams and ECC beams increase even if the load does not increase, while  
511 deflections of hybrid reinforced beams increase with the increase of loading.
- 512 • For specimens with the same nominal reinforcement ratio converted by elastic modulus ratio,  
513 ultimate moment increases with the decrease of nominal reinforcement ratio converted by strength  
514 ratio. For specimens with similar nominal reinforcement ratio converted by strength, yield  
515 moment decreases with the decrease of nominal reinforcement ratio converted by elastic modulus  
516 ratio.
- 517 • For the hybrid reinforced concrete beams, the number of cracks increases while the average crack  
518 spacing and crack width decrease with increasing the height replacement ratio. The maximum  
519 crack width of specimens decrease with the increase of the height replacement ratio, regardless of

520 the reinforcement used.

- 521 • The energy dissipation of reinforced ECC beams is higher than that of reinforced concrete beams  
522 and composite beams as the ultimate compressive strain of ECC is higher than that of concrete.  
523 Energy dissipation of steel reinforced beams and hybrid reinforced beams are higher than that of  
524 FRP reinforced beams.
- 525 • For specimens with similar practical reinforcement ratio, the ductility of hybrid reinforced beams  
526 is higher than that of reinforced concrete beams. For specimens with the same nominal  
527 reinforcement ratio converted by elastic modulus ratio, ductility increases with the increase of  
528 nominal reinforcement ratio converted by strength ratio.

## 529 **Acknowledgement**

530 The authors appreciate the support of the National Natural Science Foundation of China  
531 (51678514, 51308490), the Natural Science Foundation of Jiangsu Province, China (BK20130450),  
532 Six Talent Peaks Project of Jiangsu Province (JZ-038, 2016), Graduate Practice Innovation Project of  
533 Jiangsu Province (SJCX17-0625), the Jiangsu Government Scholarship for Overseas Studies and  
534 Top-level Talents Support Project of Yangzhou University.

## 535 **References**

- 536 ACI (American Concrete Institute). (2004). "Guide test methods for fiber reinforced polymers  
537 (FRPs) for reinforcing or strengthening concrete structures." *ACI 440.3R-04*, Farmington Hills,  
538 MI.
- 539 Aiello, M. A., & Ombres, L. (2000). "Load-deflection analysis of FRP reinforced concrete flexural  
540 members." *J. Compos. Constr.*, 4(4), 164-171.

541 Aiello, M. A., & Ombres, L. (2002). "Structural performances of concrete beams with hybrid  
542 (fiber-reinforced polymer-steel) reinforcements." *J. Compos. Constr.*, 6(2), 133-140.

543 Cai, J., Pan, J., & Zhou, X. (2017). "Flexural behavior of basalt FRP reinforced ECC and concrete  
544 beams." *Constr. Build. Mater.*, 142, 423-430.

545 Chinese National Standard. (2002). "Standard for test method of mechanical properties on ordinary  
546 concrete." *GB/T 50081-2002*, China Building Industry Press, Beijing (in Chinese).

547 Chinese National Standard. (2010). "Code for design of concrete structures." *GB 50010-2010*, China  
548 Building Industry Press, Beijing (in Chinese).

549 Ge, W., Zhang, J., Cao, D., & Tu, Y. (2015). "Flexural behaviors of hybrid concrete beams  
550 reinforced with BFRP bars and steel bars." *Constr. Build. Mater.*, 87, 28-37.

551 Ge, W., Ashour, A. F., Ji, X., Cai, C., & Cao, D. (2018). "Flexural behavior of ECC-concrete  
552 composite beams reinforced with steel bars." *Constr. Build. Mater.*, 159, 175-188.

553 Grace, N. F., Sayed, G. A., Soliman, A. K., & Saleh, K. R. (1999). "Strengthening reinforced  
554 concrete beams using fiber reinforced polymer (FRP) laminates." *J. ACI Struct.*, 188(8),  
555 865-875.

556 Gravina, R. J., & Smith, S. T. (2008). "Flexural behaviour of indeterminate concrete beams  
557 reinforced with FRP bars." *Steel Constr.*, 30(9), 2370-2380.

558 Kara, I. F., Ashour, A. F. & Koroğlu, M. A. (2015). "Flexural behavior of hybrid FRP/steel reinforced  
559 concrete beams." *Compos. Struct.*, 129, 111-121.

560 Lau, D., & Pam, H. J. (2010). "Experimental study of hybrid FRP reinforced concrete beams." *Eng.*  
561 *Struct.*, 32(12), 3857-3865.

562 Leung, H. Y. & Balendran, R. V. (2003). "Flexural behaviour of concrete beams internally  
563 reinforced with GFRP rods and steel rebars." *Struc. Surv.*, 21(4):146-157.

564 Maalej, M., & Leong, K. S. (2005). "Engineered cementitious composites for effective  
565 FRP-strengthening of RC beams." *Compos. Sci. Technol.*, 65(7), 1120-1128.

566 Maalej, M., & Li, V. C. (1995). "Introduction of strain hardening engineered cementitious composites  
567 in design of reinforced concrete flexural members for improved durability." *J. ACI Struct.*,  
568 92(2), 167-176.

569 Maalej, M., Quek, S. T., Ahmed, S. F. U., Zhang, J., Lin, V. W. J., & Leong, K. S. (2012). "Review  
570 of potential structural applications of hybrid fiber engineered cementitious composites." *Constr.*  
571 *Build. Mater.*, 36(11), 216-227.

572 Masmoudi, R., Thériault, M., & Benmokrane, B. (1998). "Flexural behavior of concrete beams  
573 reinforced with deformed fiber reinforced plastic reinforcing rods." *J. ACI Struct.*, 95(6),  
574 665-676.

575 Pecce, M., Manfredi, G., & Cosenza, E. (2000). "Experimental response and code models of GFRP  
576 RC beams in bending." *J. Compos. Constr.*, 4(4), 182-190.

577 Qu, W., Zhang, X., & Huang, H. (2009). "Flexural behavior of concrete beams reinforced with hybrid  
578 (GFRP and steel) bars." *J. Compos. Constr.*, 13(5), 350-359.

579 Soric, Z., Kisicek, T., & Galic, J. (2010). "Deflections of concrete beams reinforced with FRP bars."  
580 *Mater. Struct.*, 43(1), 73-90.

581 Tu, Y., Zhang, J., & Qian, Y. (2009). "Experimental and theoretical investigation of flexural  
582 load-carrying capacity of concrete beams reinforced with AFRP tendons." *J. Southeast Univ.*  
583 *(Nat. Sci.), China*, 39(3), 563-568.

- 584 Wang, S., Wu, C., & Li, V. C. (2001). "Tensile strain-hardening behavior of polyvinyl alcohol  
585 engineered cementitious composite (PVA-ECC)." *J. ACI Mater.*, 98(6), 483-492.
- 586 Xu, S. L., & Li, Q. H. (2009). "Experimental investigation and analysis on flexural performance of  
587 functionally graded composite beam crack-controlled by ultrahigh toughness cementitious  
588 composites." *Sci, China Ser, E.*, 52(6), 1648-1664.
- 589 Xu, S., Wang, N. & Li, Q. (2010). "Experimental study on the flexural performance of concrete beam  
590 strengthened with ultra high toughness cementitious composites." *J. Civil. Eng., China*, 43 (5):  
591 17-22.
- 592 Xu, Y., & Pan, J. (2013). "Flexural behaviors of double-reinforced ECC beams." *J. Southeast Univ.*  
593 *(Eng. Ed.)*, China, 29(1): 66-72.
- 594 Yuan, F., Pan, J., & Leung, C. K. Y. (2013). "Flexural behaviors of ECC and concrete/ECC  
595 composite beams reinforced with basalt fiber-reinforced polymer." *J. Compos. Constr.*, 17(5),  
596 591-602.
- 597 Yuan, F., Pan, J. L., & Wu Y. F. (2014). "Numerical study on flexural behaviors of steel reinforced  
598 engineered cementitious composite (ECC) and ECC/concrete composite beams." *Sci. China*  
599 *Technol. Sc.*, 57(3), 637-645.
- 600 Zhang, X., Xu, S., & Li, H. (2010). "Theoretical analysis of flexural performance of plain concrete  
601 composite beams strengthened with ultrahigh toughness cementitious composite." *J. Civil Eng.,*  
602 *China*, 43(7), 51-62.
- 603 Zhang, J., Leung, C. K. Y., & Yin, N. C. (2006). "Flexural performance of layered ECC-concrete  
604 composite beam." *Compos. Sci. Technol.*, 66(11-12), 1501-1512.